NASA TECHNICAL NOTE

NASA TN D-2464

NASA TN D-2464

INVESTIGATION OF THERMAL SHOCK RESISTANCE OF ZIRCONIA WITH METAL ADDITIONS

by Alan Arias

Lewis Research Center
Cleveland, Ohio

NATIONAL AERONAUTICS AND SPACE ADMINISTRATION • WASHINGTON, D. C. • SEPTEMBER 1964

INVESTIGATION OF THERMAL SHOCK RESISTANCE OF ZIRCONIA WITH METAL ADDITIONS

By Alan Arias

Lewis Research Center
Cleveland, Ohio

NATIONAL AERONAUTICS AND SPACE ADMINISTRATION

For sale by the Office of Technical Services, Department of Commerce,
Washington, D.C. 20230 -- Price $2.00

CONTENTS

INTRODUCTION

Zirconium oxide or zirconia has a melting point of about 2700° C, is resistant to chemical attack by acids and bases, is very stable at high temperatures in oxidizing atmospheres, and is inert when in contact with most metals at high temperatures. In addition, zirconia is relatively inexpensive and abundant. These characteristics of zirconia would make it a very satisfactory material for many high-temperature applications, were it not for the fact that pure zirconia undergoes an allotropic transformation from tetragonal to monoclinic on cooling through a temperature range in the neighborhood of 900° C. This transformation takes place with a volume increase of about 3 percent. During the reverse transformation near 1100° C on heating, zirconia shrinks by about the same amount. The large anisotropic volume changes associated with the transformation cause bodies made from pure zirconia to disintegrate during their manufacture or when in use. In practice, this difficulty is circumvented by adding small amounts of certain oxides, such as calcia, magnesia, yttria, etc., to zirconia (~~refs. 1 to 3~~). Depending on the kind and amount of oxide added to the zirconia, the high-temperature crystal structure of the combination is totally or partially retained on cooling, and the allotropic transformation is also totally or partially suppressed. This so-called stabilized zirconia performs satisfactorily in many high-temperature applications, but the addition of stabilizing oxides also introduces some undesirable features, such as an increase in the thermal-expansion coefficient, a lowering of the melting point, and, for some types of stabilized zirconia, a tendency to disintegrate on prolonged thermal cycling (~~refs. 4 and 5~~). A zirconia-base material combining the high-temperature properties of pure zirconia without the disadvantages associated with the use of stabilizers would be highly desirable.

References 2 and 6 reported making bodies of zirconia with titanium additions without the benefit of stabilization. One of the most intriguing characteristics of these zirconia-titanium compositions is their reportedly good thermal shock resistance despite the fact that the thermal-expansion-temperature curve for these compositions (~~ref. 2~~) is similar to that of pure zirconia (~~ref. 4~~). Unfortunately, no quantitative data on the thermal shock resistance of the zirconia-titanium compositions are available. In addition, the reasons why titanium additions improve the thermal shock resistance of zirconia are not clear despite some reported research in this direction.

It has been surmised that the improved thermal shock resistance of the zirconia-titanium material is due to the nonstoichiometry of the zirconia in these compositions (~~ref. 6~~). In another report, the improvement in thermal shock resistance has also been ascribed to the ability of the metal particles to relieve stress concentrations (ref. 7). The high-temperature reactions of zirconia with titanium were investigated (ref. 8) and the increased thermal shock resistance of zirconia with titanium additions was attributed to the substitutional solid solution of titanium in zirconia. Some low-temperature ductility and low-temperature creep for the zirconia-titanium material were reported, and it is surmised that this ductility accounts for the improvement in thermal shock resistance (ref. 9). Although references 6 to 9 are not necessarily contradictory, it is difficult to conceive a coherent theory to explain the effects of titanium additions on the thermal shock resistance of zirconia.

The very fact that although this material undergoes about the same volumetric change as pure zirconia during the allotropic transformation and yet can be cycled through the transformation range without cracking clearly indicates the presence of some thermal-shock-resisting mechanism the elucidation of which and possible applicability to other ceramic materials is worthwhile investigating. The elucidation of this thermal-shock-resisting mechanism together with the quantitative evaluation of the thermal shock resistance of the zirconia with 15 mole percent titanium compositions pioneered in reference 7 is the main objective of the present investigation.

The approach used in this investigation follows this sequence:

(1) Quantitative evaluation of the thermal shock resistance of zirconia with 15 mole percent titanium

(2) Determination of the physical properties of zirconia with 15 mole percent titanium that influence its thermal shock resistance

(3) Comparison of experimental (step 1) and calculated (step 2) thermal shock resistances

(4) Elucidation of the mechanism by which titanium improves the thermal shock resistance of zirconia

In the first part (part (1)), the thermal shock resistance of zirconia with 15 mole percent titanium is determined as a function of quench severity by the method of reference 10, where disks with thermally insulated faces are quenched from successively higher temperatures in a medium of fixed quench severity until the disks crack. The maximum temperature difference ΔT that the disk is capable of withstanding without cracking under a specified quench severity - defined as the product of the maximum radius of the disk r_m and the surface heat-transfer coefficient h - is usually taken as a measure of the thermal shock resistance of the material (refs. 11 and 12). In this manner, the thermal shock resistance of different materials at any given quench severity can be compared. In this part, comparison is made between the thermal shock resistance of zirconia with 15 mole percent titanium prepared by three different methods with that of calcia-stabilized zirconia.

The second part (part (2)) deals with the determination of some physical properties of the zirconia with 15 mole percent titanium. The reason for this part of the investigation is that the thermal shock parameter ΔT can be shown to be a function not only of shape and quench severity but also of the strength σ, modulus of elasticity E, coefficient of thermal expansion α, thermal conductivity k, and (for some shapes) Poison's ratio ν (refs. 11 and 12). Except for Poisson's ratio, all these properties are determined as a function of temperature from room temperature to above the transformation range. In addition, the heat capacity of this composition is also determined because it is used in connection with the determination of h in part (1) of this report.

The third part (part (3)) deals with the comparison of the experimental thermal shock resistance of the zirconia-titanium composition in the first part

(part (1)) with the calculated thermal shock resistance obtained from the data determined in the second part (part (2)). From this comparison and from the comparison between the experimental thermal shock resistances of zirconia with 15 mole percent titanium and stabilized zirconia, the factors that influence the increase in the thermal shock resistance of zirconia due to titanium additions are surmised.

The fourth part (part (4)) deals with additional experiments carried out to verify the conclusions of the preceding third part and to elucidate further the role played by titanium in improving the thermal shock resistance of zirconia.

Other sections of this report deal with sample preparation, equipment, and procedures. Most of the equipment used in this investigation was designed by the author, and the novel characteristics of these apparatus are fully described either in the text or in the appendixes. Some of the procedures are also described in the appendixes.

MATERIALS AND SPECIMEN PREPARATION

Raw Materials

The most important raw materials used in this investigation are shown in table I together with their typical analysis and particle sizes when known.

Sample Preparation

Weighing. - All materials were dried in a vacuum desiccator prior to weighing. All weighing was carried out on balances that would ensure an accuracy of 0.01 percent or better.

Mixing. - Some compositions were dry mixed in V-blenders provided with intensifiers for at least 15 minutes, after which time 5 percent by weight of water was added as a temporary binder and mixing was continued for another 15 minutes.

Milling. - Milling was carried out in 2-liter-capacity 12.5-centimeter inside-diameter tungsten-carbide (with 6 percent cobalt) mills. All milling was done with 400-gram batches of material by using 4 kilograms of tungsten-carbide (with 6 percent cobalt) balls and 1 liter of technical grade acetone as the grinding media. All the compositions designated as-milled were milled at 80 rpm for 72 hours. After milling, the acetone was removed by evaporation in a stream of warm air. After removal of the acetone, the compositions were mixed with 5 weight percent of water in cone blenders (provided with intensifiers) for 15 minutes.

Pickup on milling. - Colorimetric chemical analysis of the milled compositions showed a maximum of 0.37 weight percent tungsten (and corresponding amounts of carbon and cobalt) picked up on milling.

Particle size analysis. - Particle size analysis by the B.E.T. method gave an average particle size of 0.14 micron for milled zirconia with 15 mole percent titanium, compared with an average particle size of 0.25 micron for the mixed materials. These values correspond to specific surface areas of 3.74 and 2.07 square meters per gram, respectively.

Cold-pressing. - Bar specimens were cold-pressed in split steel dies at pressures between 10,000 and 20,000 psi. Disk and cylindrical specimens were cold-pressed in double-acting steel dies at 20,000 psi.

The cold-pressed specimens were placed inside plastic tubing, which was then evacuated and heat-sealed gas tight. Usually about a dozen specimens were sealed simultaneously in the same piece of tubing. The plastic sealed specimens were pressed hydrostatically at 46,000 to 50,000 psi. After pressing, the plastic tubing was slit open, the specimens removed and then dried in a vacuum desiccator at 60° to 80° C for 24 hours.

Sintering. - With pure zirconia and zirconia-metal mixtures, all sintering was carried out in induction-heated vacuum furnaces. The specimens, either bars, disks, or cylinders, were sintered several at a time in tungsten sintering boats, such as the one shown in figure 1. The sintering boat or sample

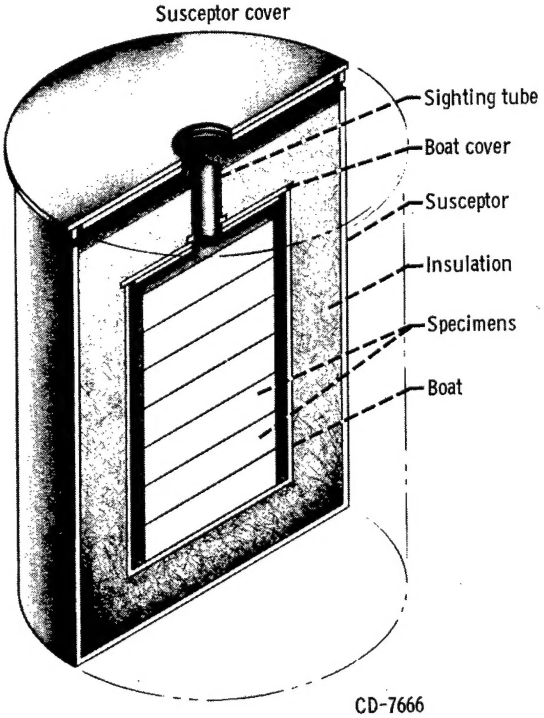

Figure 1. - Tungsten sintering boat.

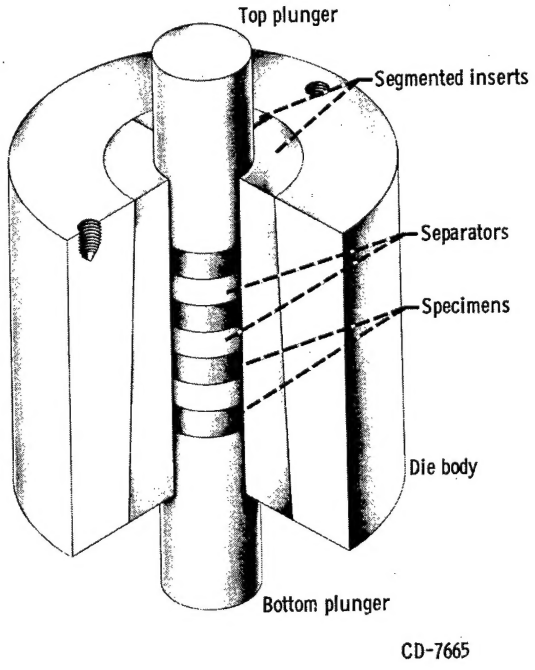

Figure 2. - Hot-pressing graphite die.

holder proper is located inside the cylindrical susceptor and thermally insulated from it by zirconia of the same composition as that of the specimens being sintered. This type of sintering boat was used in order to minimize the

danger of thermally shocking the specimens during heating or cooling.

Unless stated otherwise, all vacuum sintering was carried out at 1870°±30° C for 1 hour at pressures of less than 0.5 micron of mercury throughout the run. The temperature was measured by a disappearing-filament optical pyrometer. The pressure was measured with an ionization gage.

The requirement that the pressure should not exceed 0.5 micron of mercury lengthened the sintering runs made with milled compositions, since these compositions degassed considerably at low temperatures (<500° C). This degassing is attributed to some organic compound formed from the acetone during milling, but no attempt has been made to identify it.

Disks and bars of calcia-stabilized zirconia were also made for comparison purposes. These specimens were made from Zircoa B from the Zirconium Corporation of America. This material was milled and cold-pressed into bars and disks by the procedures indicated. Sintering was carried out by the Zirconium Corporation of America in air furnaces at 1800° C for 3 hours.

Hot-pressing. - Some compositions were hot-pressed in vacuum. A typical graphite die used for hot-pressing disks is shown in figure 2. This die is double acting and features a segmented conical insert to facilitate removal of the hot-pressed disks. Usually, four disks were hot-pressed simultaneously by placing graphite separators between the specimens. A similar die was used for making test bars.

Hot-pressing was carried out in the furnace shown in figure 3, which has already been described in the literature (ref. 13).

Disks of zirconium oxide with 15 mole percent titanium were made by hot-pressing the mixed raw materials at 1600°±50° C for 1 hour under a pressure of 2000 to 2100 psi. Vacuum was at 20 microns or less. Some disks and bars of pure zirconium oxide (CP Zirox, table I) were also hot-pressed at 2025°±40° C for 1 hour under a pressure of 2000 to 2100 psi and vacuums of 30 microns of mercury or less. Invariably, the hot-pressed specimens were covered with a thin layer of zirconium carbide that was completely removed on grinding the specimens to size.

Grinding and polishing. - Disks and bars were ground all over to the required sizes by using diamond wheels with an abundant supply of coolant. All ground specimens had a surface finish of 50 microinches or better. All sharp edges in disks and bars were given a radius of about 0.005 inch. As will be indicated in the proper places, some of the bars were polished to a mirror finish with diamond powder.

Sample inspection. - All ground specimens were tested for cracks and pinholes by means of die penetrant. Those specimens showing defects were discarded.

Composition and designation of samples. - The various compositions made were designated by means of letters and numbers intended to indicate composi-

tion and processing. For the ceramic-metal compositions, the first letter indicates the oxide (Z for zirconia, H for hafnia), the second letter indicates the metal additive (T for titanium, etc.), the number indicates the mole percent of metal, and the last letter or group of letters indicates the processing

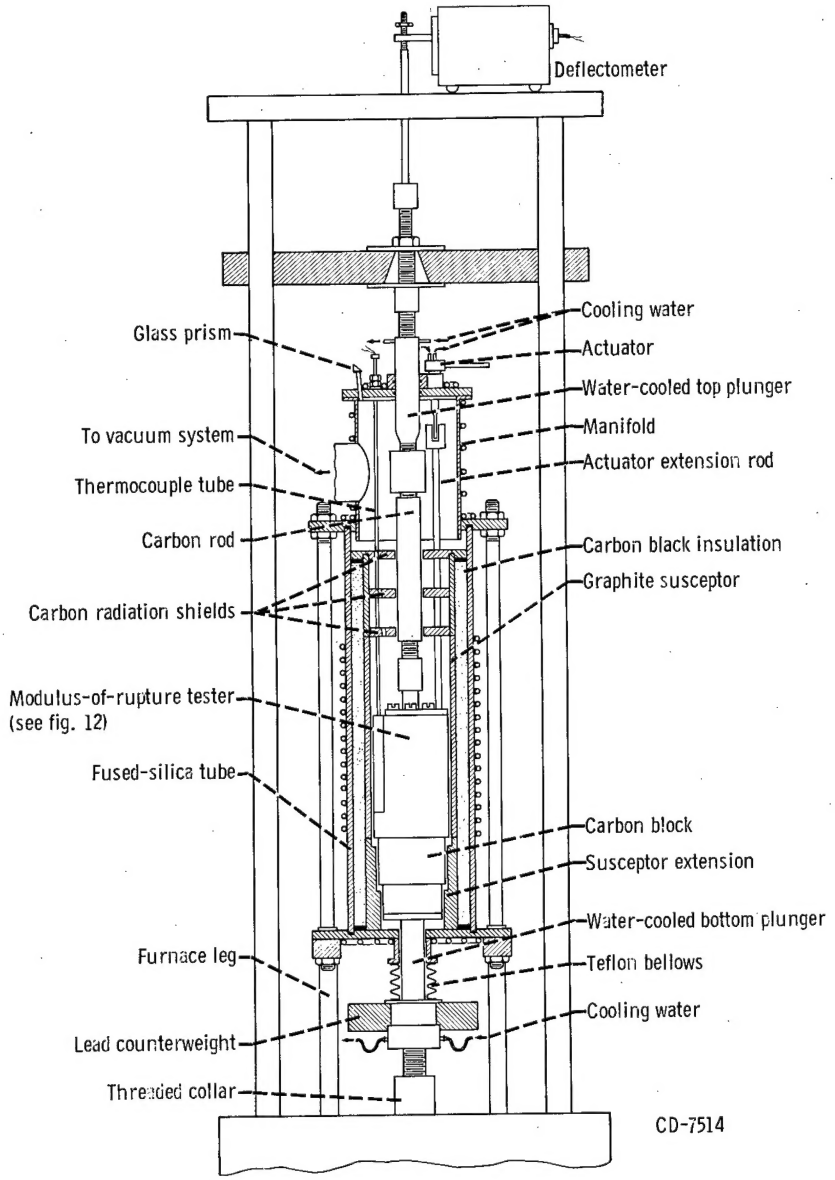

Figure 3. - High-temperature vacuum furnace.

(M for milled, HP for hot-pressed). These compositions and their designations are shown in table II together with a brief description of the processing treatment.

Metallography. - Most of the compositions were examined metallographically for porosity, structure, and grain size. Standard methods of polishing and etching were used.

Density. - The densities of the samples were determined by water immersion.

EXPERIMENTAL PROCEDURES

Experimental Thermal Shock Resistance

Apparatus and procedure. - The apparatus used for the determination of thermal shock resistance was designed by the author and is shown in figure 4. For purposes of explanation, this apparatus will be divided into three parts: a heating chamber, a sample carrier, and a quenching chamber.

The heating chamber is an Inconel tube about 2 inches inside diameter that fits into the hole of a vertical tube furnace. The heating chamber is secured to the furnace by a bottom plate and a collar. This heating chamber is provided with a bottom flange on which the quenching chamber is screwed. The cover for the heating chamber has a center hole through which the stem of the sample holder passes. This opening is made gas tight by means of an O-ring. The cover is also provided with an inert gas inlet, a silicone rubber gasket, and means of securing the cover to the Inconel tube. The inert gas outlet is located at the bottom of the heating chamber. A trap door, normally held closed by a counterweight, reduces heat losses by radiation while the sample is being heated.

The purpose of the sample carrier is to carry the thermal shock specimen from the heating chamber to the quenching chamber. The thermal shock specimens are disks 1.375±0.002 inches outside diameter and 0.312±0.002 inch thick. The faces of the thermal shock specimen are insulated by ceramic fiber paper rings and disks backed by fused-silica disks of the same diameter as the sample and located so as to form a dead air space between the sample and the ceramic fiber disks. When water or other liquid is used as a quenching medium, either silicone rubber or rubber impregnated asbestos is used instead of ceramic fiber as gasketing material. The upper silica and ceramic fiber insulating rings have holes through which thermocouples can reach the surface of the specimen for temperature measurements. This assembly of sample and insulating disks is held in place by two short pieces of Inconel tubing, also of the same outside diameter as the sample, which, in turn, are held between the top and bottom Inconel plates of the sample carrier. The top plate is provided with a center hole for the passage of the thermocouples and is welded to an Inconel tube or stem. The bottom plate is kept in position by four 0.032-inch-diameter tungsten wires, which are held in tension by a tension plate and a high-temperature spring attached to the stem of the sample carrier. The wires pass through center holes in adjusting screws secured to the tension plate. These screws are used to equalize the tension in the wires. Tightening is accomplished by a knurled nut, which is also the lower race of a ball bearing. The upper race of this ball bearing is a plate on which the high-temperature spring rests. Threaded ceramic disks (lava stone, ceramic fiber board, etc.) below the knurled nut prevent overheating of the spring and reduce heat losses. The thermocouples reach the exterior of the assembly through the center hole in the stem. The sample carrier can be kept in position by tightening the collar in the cover or

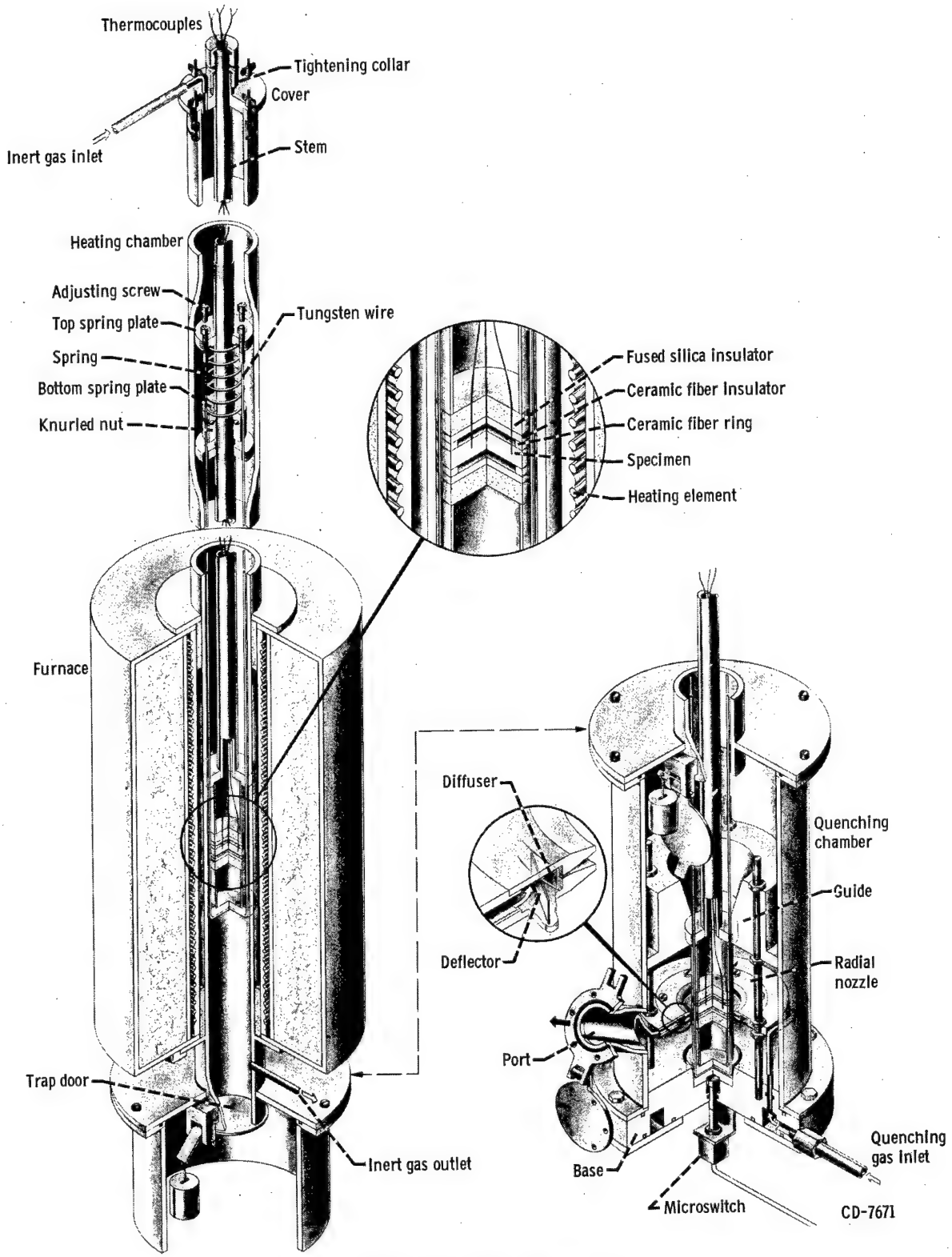

Figure 4. - Thermal shock apparatus.

by rods of suitable length between the protruding portion of the stem and the cover.

The quenching tank is attached to the lower flange in the heating chamber by screws. The cooling gas enters the tank through the base where a manifold distributes the gas evenly among six tubes leading to the nozzle. The gas entering the manifold in the nozzle is deflected by vanes located in front of the gas ports. A perforated plate or wire cloth acts as a diffuser to even out the flow in the nozzle. The nozzle is held in place by three rods screwed to the base, which also support the guide. The whole assembly is made gas tight by gaskets.

The left portion of figure 4 shows the specimen in the heating position. After the specimen reaches the desired equilibrium temperature, the sample holder is allowed to drop into the quenching tank by loosening the collar in the cover. As the sample holder falls, it opens the trap door in the bottom of the heating tube, passes through the guide, and comes to rest in a recess in the base of the quenching tank. As the specimen holder enters this recess in the base, it actuates a microswitch that sets the temperature-recorder-chart motor in motion and opens a solenoid valve in the inlet to the quenching tank. Manual switches for the solenoid valve and recorder motors override the microswitch and allow adjustment of gas flow and chart position before the quenching run is started. The quenching gas leaves the chamber through a side port in the cover. This side port has a gasketed lid that can be kept closed until the quenching run starts. It should be noted that the system is gas tight and, consequently, could be used for testing hazardous materials.

The gases used for cooling the test specimens were either air or helium. Helium was obtained from helium bottles connected in parallel. Pressure was held constant by two pressure regulators connected in series and was measured by a water manometer. Air of up to 120 psi was obtained from the service line. Before entering the quenching tank, this air was passed through filters and through a pressure regulator.

In order to quench in water, the quenching chamber was removed and the specimen carrier was dropped directly into a vessel of water. During these runs, the temperature recorders were started with the override switch.

Some mild quenches were obtained by cooling the specimens in the lower portion of the heating tube. The heat-transfer coefficient could be varied slightly by closing the quenching chamber port and flowing gas either upward or downward through the tube. This was the method used for quenching through the transformation temperature. Although the same results could have been obtained by quenching specimens of smaller radii in the quenching chamber, this would have required regrinding specimens already available and a redetermination of the heat-transfer coefficient as a function of r_m and gas pressure. In addition, the sample carrier would have had to be modified to accommodate the new size of specimen. For this investigation, direct cooling in the lower portion of the heating tube was more expedient.

In order to determine ΔT, a series of quenching experiments with constant cooling gas pressure and variable initial temperature was carried out. A

typical test procedure was as follows: The furnace temperature controller was adjusted to the desired temperature, the specimen holder position was adjusted so that the specimen was in the center of the hot zone in the heating chamber, and the specimen was allowed to reach equilibrium temperature. Heating was always carried out in an argon atmosphere with an argon pressure of 1 inch of water above atmospheric pressure.

Just before quenching, the cooling gas pressure was adjusted to the desired value. The specimen holder was then dropped into the quenching chamber and allowed to cool to about one-third of the initial temperature before stopping the gas flow. The specimen holder was then removed from the thermal shock apparatus and the specimen examined for cracks at a magnification of 5.

If the specimen was sound, it was reheated in the same manner but to a temperature about 10 percent higher than before, and the quenching experiment repeated at the same gas pressure. The specimen was again examined for cracks.

This procedure was repeated until the specimen cracked. The average temperature between this run and the previous run, minus the temperature of the cooling gas gave ΔT

$$\Delta T = \frac{T_1 + T_2}{2} - T_f \qquad (1)$$

where

T_1 initial temperature in run before cracking

T_2 initial temperature in run where cracking took place

T_f final temperature of specimen (temperature of quenching medium)

For quenches through the transformation temperature of zirconia, the procedure was to quench the specimen in successively lower portions of the heating tube until the specimen cracked. In order to determine the final temperature T_f, the specimen was allowed to remain in the quenching position for at least 1 hour, and the temperature was determined by thermocouples attached to the upper face of the specimen. During these runs, the specimens were always heated to 1180° C and quenched from this temperature, but the initial temperature was taken as that corresponding to the start of the transformation on cooling (900° C). The reason for using this initial temperature is that the coefficient of thermal expansion changes so radically in this temperature range that it overrides all other considerations. In other words, it would not make any difference whether the specimen is quenched directly from 1180° C or is cooled first from 1180° to 900° C, for instance, and then quenched under the same h and T_f. For this type of quench, ΔT was taken as 900° C - T_f.

Heat-transfer coefficient. - The surface heat-transfer coefficient h as a function of gas pressure was determined in the same apparatus described for the determination of ΔT. The specimens used for the determination of h were disks of ZT-15-M (see table II) of the same dimensions as the specimens used for the determination of ΔT but with thermocouple holes 0.032 inch in diam-

eter located at relative radii r/r_m of 0, 0.5, and 0.8. The heat-transfer coefficient was determined from cooling curves, such as the ones shown in figure 5, with the aid of the plot of Russell's tables (ref. 14) shown in figure 6. The detailed procedure for the determination of h is given in appendix A.

Material Properties Determination

General considerations. - The values of the properties to be used in the thermal shock equation (refs. 10 to 12 and 15) require some explanation. For the thin disk, the thermal shock equation (ref. 10) is

$$\Delta T = \frac{\sigma_{\theta_{max}}}{E\alpha}\left(2 + 4.3\,\frac{k}{hr_m}\right) \qquad (2)$$

where $\sigma_{\theta_{max}}$ is the tangential stress at the periphery of the disk at the moment of rupture.

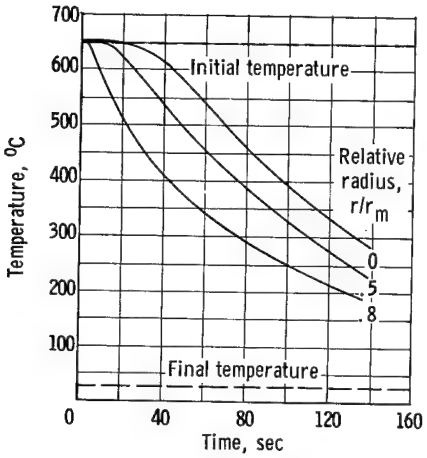

Figure 5. - Typical cooling curves for disk of zirconium oxide with 15 mole percent titanium (ZT-15-M). Quenching medium, helium at 10 inches of water.

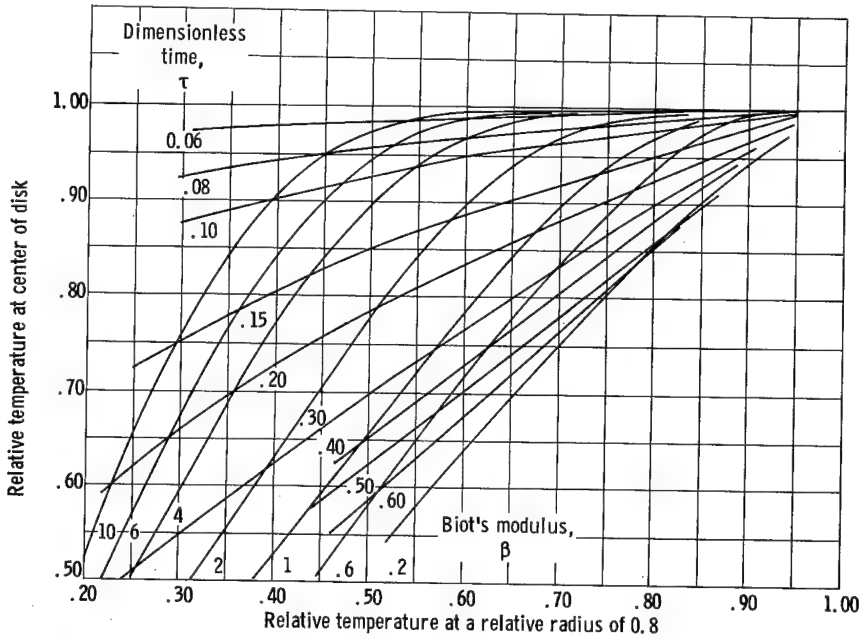

Figure 6. - Relative temperatures at relative radii of 0 and 0.8 as functions of dimensionless time and Biot's modulus.

The coefficient of linear thermal expansion α for zirconia is anisotropic (ref. 16) and, therefore, must be determined on the same kind of polycrystalline material used for making thermal shock specimens.

On thermally shocking specimens, the stresses build up relatively slowly and, consequently, the static rather than the dynamic Young's modulus of elasticity E applies.

It is known that the rupture stress of a brittle material depends on the stress distribution at the moment of rupture. Based on Weibull's statistical theory of strength, it is concluded in the analysis of reference 10 that the strength term to be used in the thermal shock equation for a thin disk is closely approximated by the modulus of rupture of a beam of rectangular cross section under four-point loading. The height of the beam should be such that the stress gradient is approximately the same as that at the surface in a thermally shocked disk at rupture. In addition, the distance between the two inner points on which the load is applied should be $2\pi r_m$ and the width of the beam should be the same as the thickness of the disk. For the reasons explained in appendix E, however, the last two conditions need to be met only approximately. For the beam, the stress gradient is

$$\frac{\partial \sigma}{\partial r} = \frac{2PX}{bd^3} = \frac{2\sigma_M}{d} \tag{3}$$

where

$\partial\sigma/\partial r$ stress gradient, lb/cu in.

P load at rupture, lb

X distance, in symmetrically loaded beam, between outer support and nearest point of application of load, in.

b width of beam, in.

d height of beam, in.

σ_M modulus of rupture, psi

The stress gradient in the disk can be obtained from the derivative with respect to r of the equation for the tangential stress for the thin disk given in reference 17. Equating the value of this derivative at $r = r_m$ to the stress gradient in equation (3) yields σ_M/d. In order to determine d for the correct stress gradient, an experimental plot of σ_M/d against d is required.

On the assumption that the distribution of defects (responsible for the variation of σ_M with dimensions) does not vary with temperature, the corresponding four-point modulus of rupture at temperature T can be determined from a modulus-of-rupture - temperature curve under three-point loading:

$$\sigma_{M_T,2} = \left(\frac{\sigma_{M_2}}{\sigma_{M_1}}\right) \sigma_{M_T,1} \tag{4}$$

where

$\sigma_{M_T,2}$ modulus of rupture at T and four-point loading

σ_{M_2} modulus of rupture at room-temperature four-point loading

$\sigma_{M_{T,1}}$ modulus of rupture at T and three-point loading

σ_{M_1} modulus of rupture at room-temperature three-point loading

There does not seem to be any reason for using a particular method of measurement in preference to another for the thermal conductivity k.

As stated in the INTRODUCTION, the experimental and calculated thermal shock resistances will be compared. The calculated value of thermal shock resistance will be based on property determinations in only the milled and sintered zirconia-titanium composition (ZT-15-M, table II). All the material properties to be evaluated in this part of the investigation are those of ZT-15-M, with the exception of the modulus of rupture, which includes ZT-15 and BM compositions also (see table II) for comparison purposes.

Heat capacity. - As a general rule, the molar heat capacities of most oxides are similar, particularly at high temperatures. If the material under study had been pure zirconium oxide with titanium additions, the heat capacity of the mixture could have been readily determined, since the heat capacities of both zirconium oxide and titanium are known (refs. 18 and 19). It has been surmised, however, that the zirconia in these compositions is nonstoichiometric (refs. 6, 20, and 21). For this reason and for completeness, heat-capacity measurements were carried out.

The apparatus used for the determination of heat capacity c_p is a modified version of a drop calorimeter and is shown in figure 7. In this investigation, the enthalpy ΔH of solid samples of ZT-15-M (see table II) was determined as a function of temperature. The heat capacity c_p was determined from the slope of the enthalpy-temperature curve. Details of the apparatus, calibration, and procedures are given in appendix B.

Thermal conductivity and thermal diffusivity. - Thermal conductivity from room temperature to about 1100° C was determined on cylinders of ZT-15-M (see table II) by the radial method. Two versions of the same apparatus (designed by author) were used: One for temperatures up to about 320° C and another for temperatures above this range. The maximum temperature capabilities of the apparatus is determined by that of the thermocouple assemblies used. The low-temperature modification of the apparatus is shown in figure 8 and the high-temperature modification in figure 9. The power supply is common to both versions of the apparatus and is shown in figure 10. A detailed description of the apparatus and the procedures is given in appendix C.

The thermal diffusivity was determined from measurements of thermal conductivity, heat capacity, and density by the equation

$$a = \frac{k}{c_p \rho} \tag{5}$$

where

a thermal diffusivity

k thermal conductivity

c_p heat capacity

ρ density

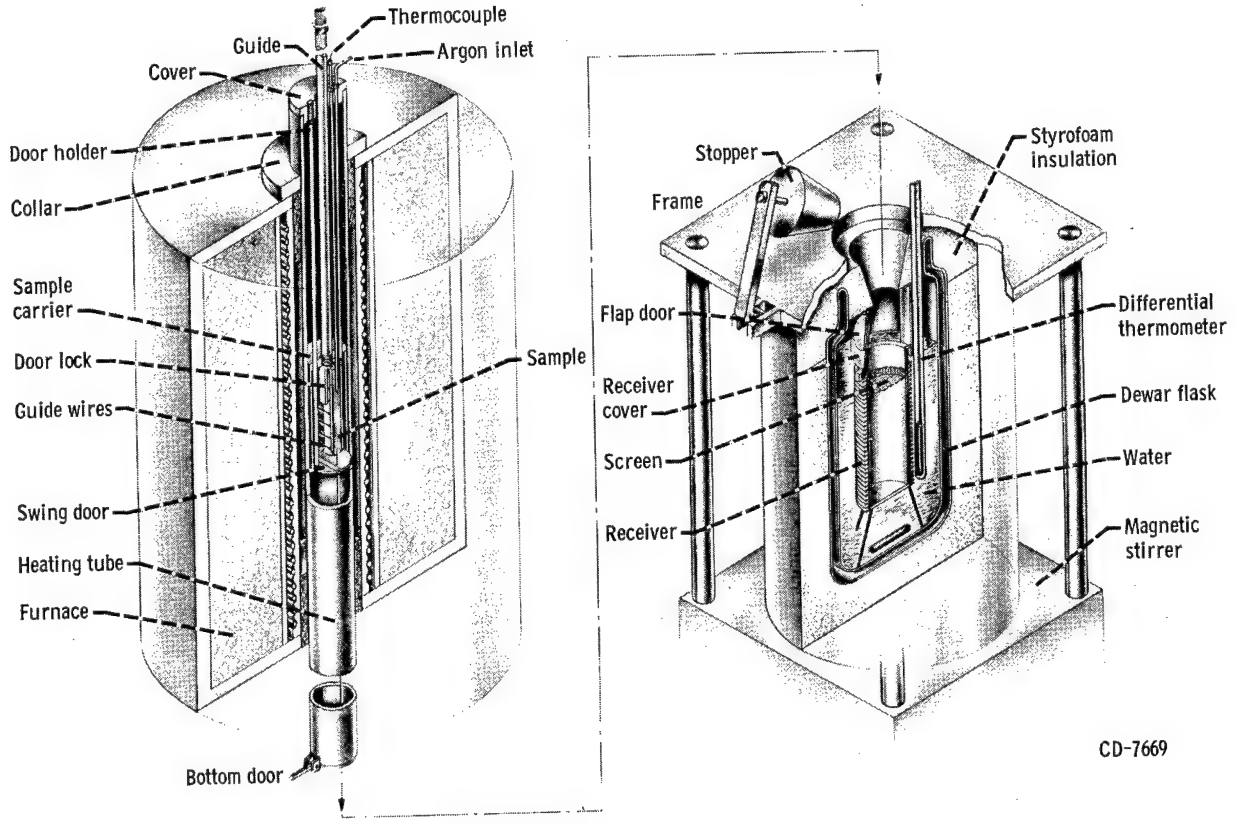

Figure 7. - Drop calorimeter.

Thermal expansion. - As already stated, the thermal expansion of zirconia with 15 mole percent titanium had already been reported in reference 22 before this investigation was started. The reported thermal expansion was obtained with a dilatometer on zirconia with 15 mole percent titanium vacuum sintered for $1\frac{1}{2}$ hours at 1870° C.

The zirconia with 15 mole percent titanium used in the present investigation was milled, cold-pressed, and sintered for 1 hour at 1870° C. As already stated, some tungsten carbide and some cobalt are picked up on milling. Because of the effect of grain size and impurities on the transformation temperature and perhaps mechanism also (refs. 16, 23, and 24), it was decided to investigate the thermal expansion of the ZT-15-M (table II) material used in the present investigation.

The vacuum dilatometer used in the present investigation was designed by the author and is shown in figure 11. This dilatometer can operate either in

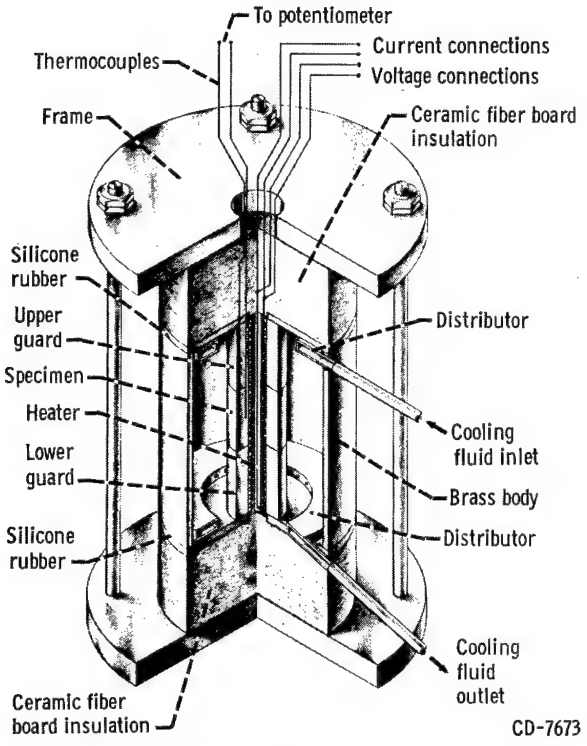

Figure 8. - Low-temperature thermal-conductivity apparatus.

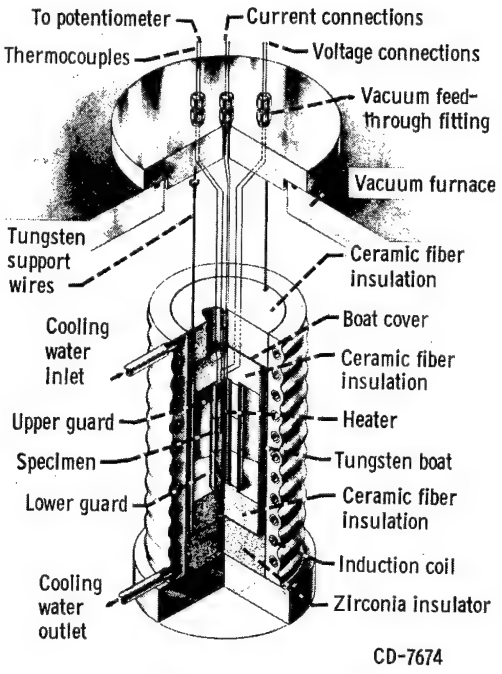

Figure 9. - High-temperature thermal-conductivity apparatus.

vacuum or inert atmospheres at temperatures in excess of 2000° C. A complete description of this dilatometer and the procedures used for determining the thermal expansion of ZT-15-M (table II) are given in appendix D.

Modulus of rupture in bending. - For the reasons already stated, the modulus of rupture rather than the tensile strength will be used in the thermal shock equation for thermal shock induced by quenching from below the transformation temperature.

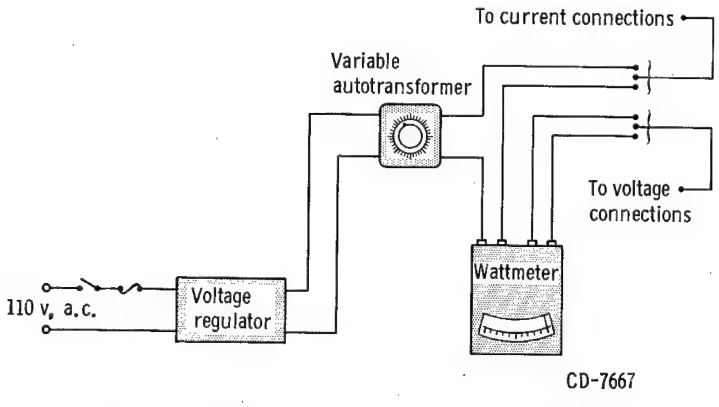

Figure 10. - Power supply for thermal-conductivity apparatus.

The modulus of rupture at room temperature both for three- and four-point loading was carried out in standard types of fixtures (ref. 25). The modulus of rupture at high temperature was carried out in vacuum in the semiautomatic modulus-of-rupture fixture shown in figure 12. This fixture and its operation have been described (ref. 13). Tests were carried out both on zirconia-titanium compositions and on calcia-stabilized zirconia. Details of the procedures used are given in appendix E.

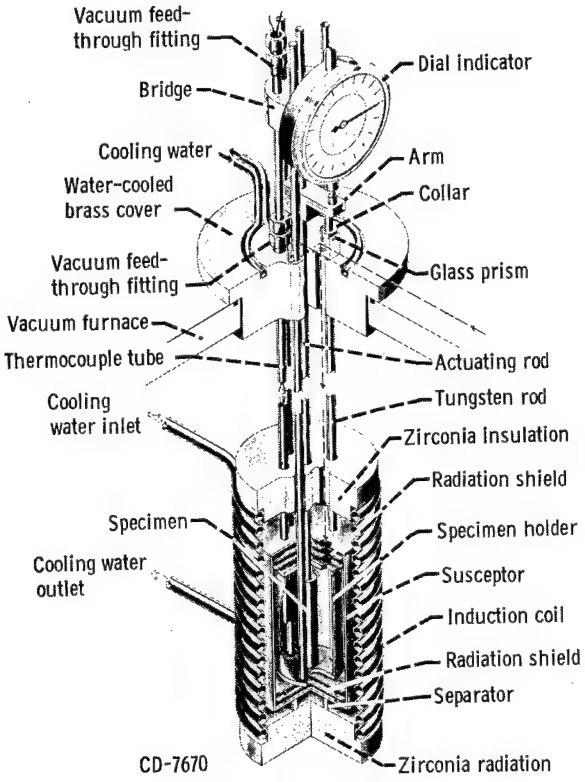

Figure 11. - Vacuum dilatometer.

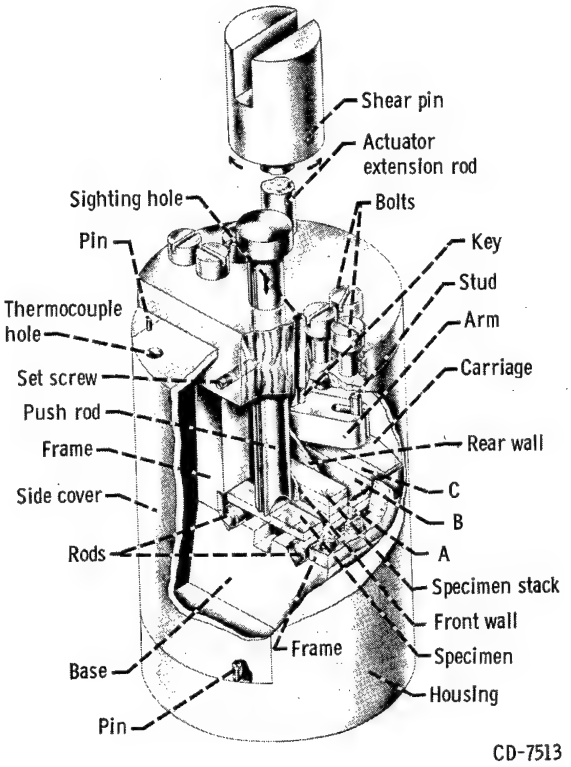

Figure 12. - Semiautomatic modulus-of-rupture tester.

Modulus of elasticity. - The modulus of elasticity for the composition designated as ZT-15-M (table II) was obtained as a function of temperature by the bending method. The modulus of elasticity in compression and Poisson's ratio were also determined at room temperature. The dynamic modulus of elasticity at room temperature was determined as a comparison of the results obtained by the bending method.

The apparatus used for determining Young's modulus of elasticity as a function of temperature by the bending method was designed by the author and is shown in figure 13. The equipment used for the modulus of elasticity in compression and for dynamic modulus of elasticity at room temperature is of standard construction. The details of all this equipment and the procedures are given in appendix F.

RESULTS

Experimental Thermal Shock Resistance

Heat-transfer coefficient for ZT-15-M. - The plots of surface heat-transfer coefficient h as a function of helium and air pressures are shown in figures 14 and 15, respectively. The values of h shown in these plots were obtained by the second method outlined in the procedure (appendix A) from the cooling curves corresponding to $r/r_m = 0.8$. The plotted values represent an

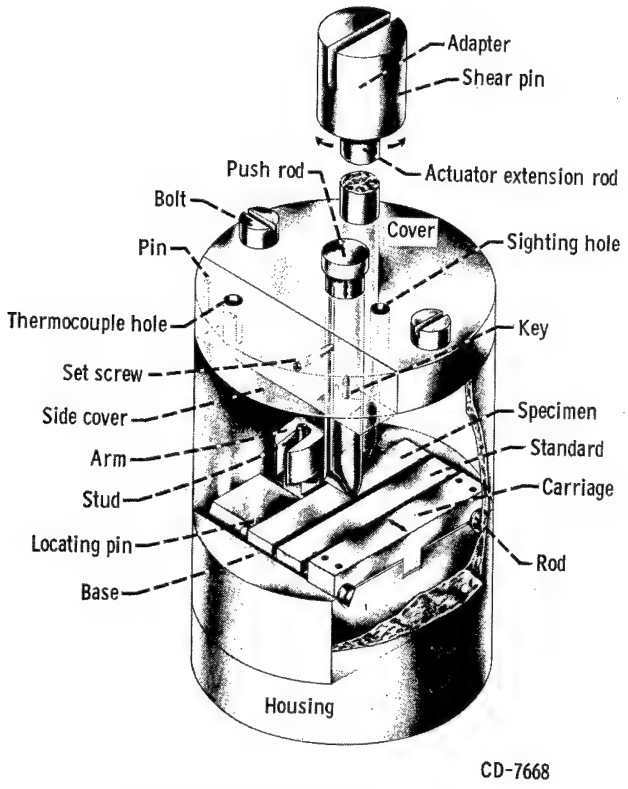

Figure 13. - Modulus-of-elasticity apparatus.

average of not less than three determinations. The values of h obtained by the first method outlined in appendix A differ from these by less than 10 percent. The value of hr_m on cooling through the transformation range was between 0.009 and 0.01 calorie per square centimeter per second per ^{o}C. This severity of quench varied slightly with the flow of argon gas used as an atmosphere, but this flow was kept constant (although of unknown magnitude) during the experiments.

The heat-transfer coefficient in boiling water was taken from the literature (ref. 10). The value of hr_m to be used in the present investigation will be 1.0 calorie per centimeter per second per ^{o}C corresponding to a value of h of 0.57 calorie per square centimeter per second per ^{o}C and $r_m = 1.745$ centimeters. Although this value of h is somewhat arbitrary, there is little error in ΔT because the curves for ΔT against hr_m from the data in the present investigation flatten out in this high range of hr_m (see figs. 16 to 18).

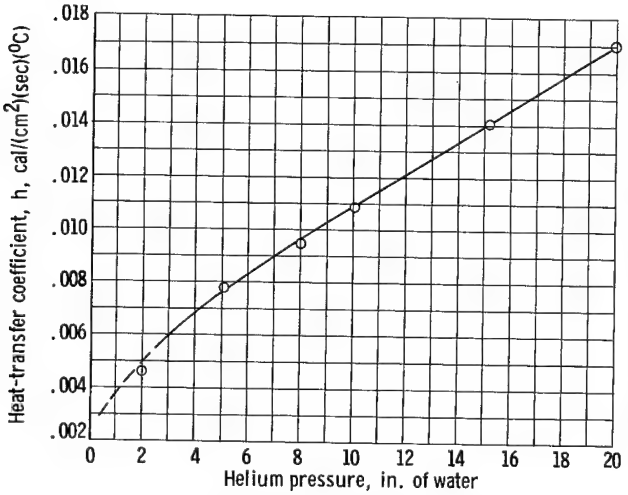

Figure 14. - Heat-transfer coefficient as function of helium pressure for disk of zirconium oxide with 15 mole percent titanium (ZT-15-M).

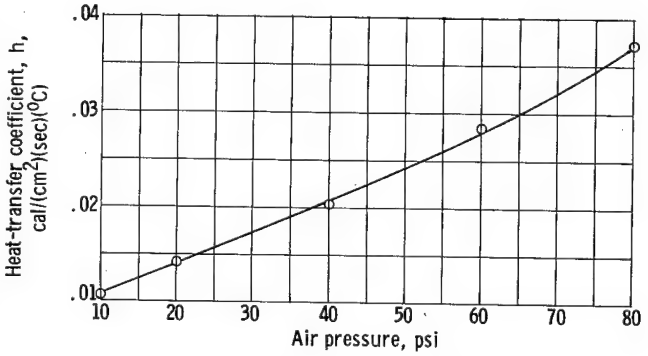

Figure 15. - Heat-transfer coefficient as function of air pressure for disk of zirconium oxide with 15 mole percent titanium (ZT-15-M).

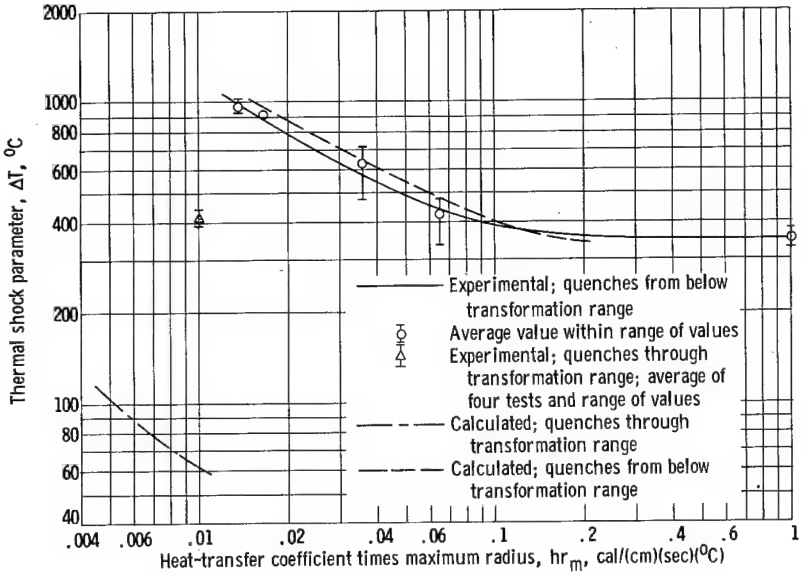

Figure 16. - Variation in maximum quenching temperature as function of heat-transfer coefficient times maximum radius for zirconium oxide with 15 mole percent titanium (ZT-15-M).

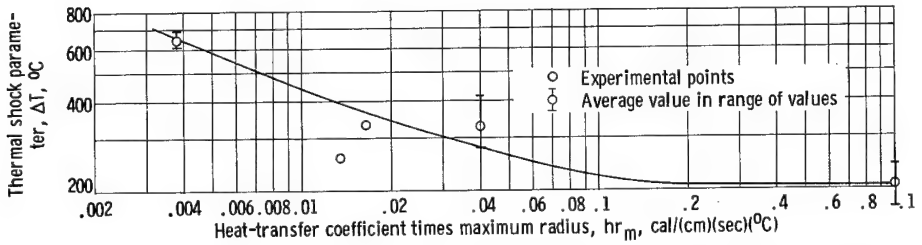

Figure 17. - Variation in maximum quenching temperature as function of heat-transfer coefficient times maximum radius for 5 weight percent calcia-stabilized zirconia.

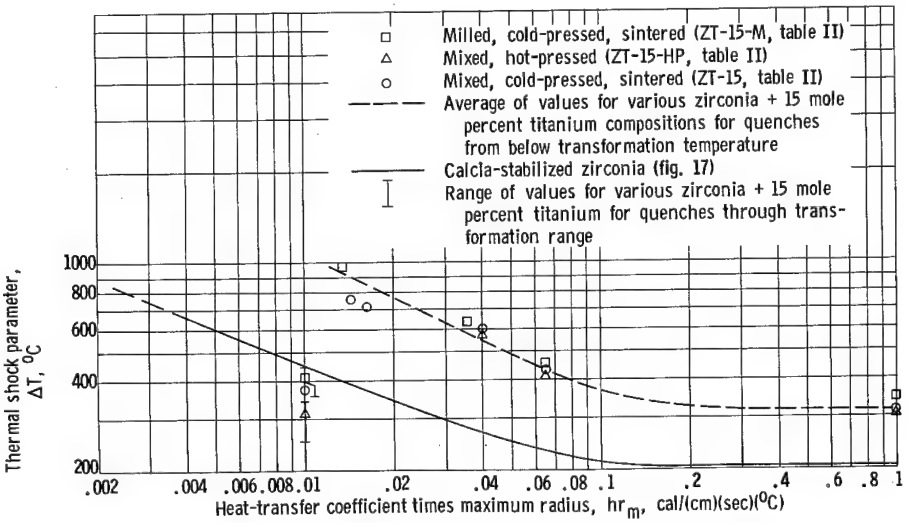

Figure 18. - Effect of processing conditions on thermal shock resistance of zirconia with 15 mole percent titanium and comparison with thermal shock resistance of calcia-stabilized zirconia.

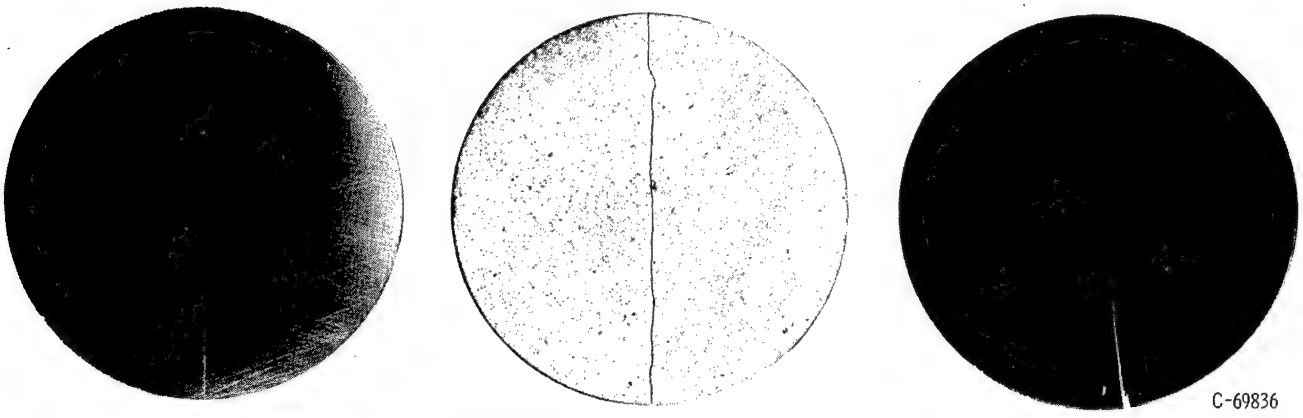

C-69836

(a) Milled zirconia with 15 mole percent titanium (ZT-15-M, table II) thermally shocked from below transformation temperature.

(b) Milled and air-sintered calcia-stabilized zirconia (BM, table II) thermally shocked.

(c) Milled zirconia with 15 mole percent titanium (ZT-15-M, table II) thermally shocked from above transformation temperature.

Figure 19. - Thermally shocked disks.

All the values of hr_m given previously will be used for all the compositions to be plotted in the present investigation. Slight variations in grain size and composition are not expected to alter h significantly.

Experimental thermal shock resistance. - The experimentally determined values of ΔT for the milled, cold-pressed, and sintered zirconia with 15 mole percent titanium (ZT-15-M) are shown plotted against hr_m in figure 16 for quenches both from below and through the transformation range. The experimentally determined curve for ΔT against hr_m for calcia-stabilized zirconia (BM, table II) is shown in figure 17. The experimentally determined curves for ΔT against hr_m for zirconia-titanium compositions designated as ZT-15, ZT-15-HP, and ZT-15-M (table II), together with the corresponding plot for stabilized zirconia (from fig. 17) are shown in figure 18. From the results shown in this figure, it is seen that the thermal shock resistance of the zirconia-titanium compositions is not appreciably affected by the different methods of preparation used in this investigation. It should be pointed out that the composition designated as ZT-15 was prepared from the same type of materials and by the same procedures used in the investigation of reference 7. Comparison of the curve for stabilized zirconia with that for the zirconia-titanium compositions shows the latter to be definitely superior for quenches from below the transformation range but slightly inferior for quenches through their transformation ranges.

A photograph of the various types of fracture of the thermally shocked disks is shown in figure 19. Thermally shocked stabilized zirconia cracks all the way through. As a general rule, the zirconia-titanium compositions crack only part way. The cracks in the specimens thermally shocked through the transformation range were invariably open, whereas those thermally shocked from below the transformation range were not.

Material Properties

Microstructures. - The microstructures of the samples prepared for this

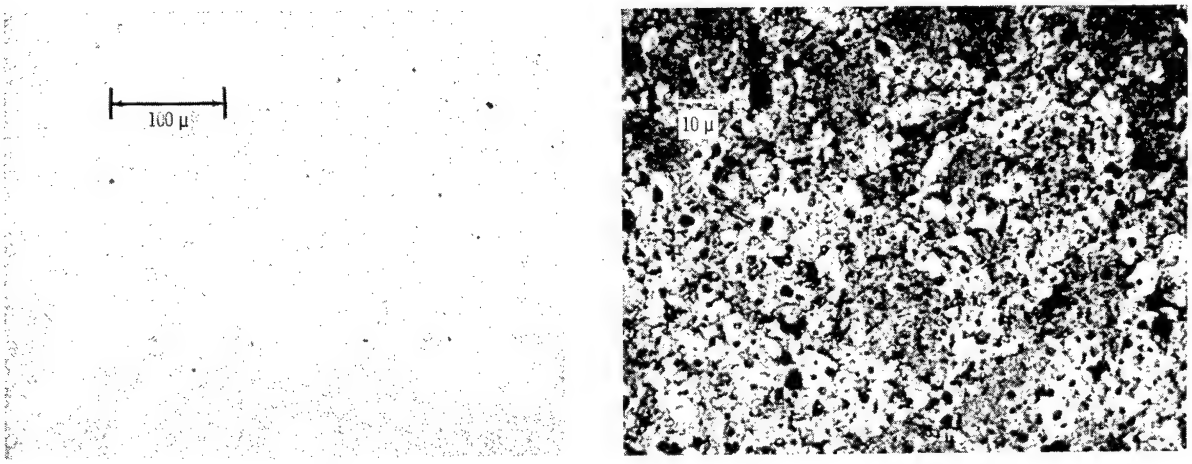

(a) Unetched. (b) Etchant, potassium bisulfate.

Figure 20. - Microstructure of zirconia with 15 mole percent titanium, milled, cold-pressed, and sintered in vacuum at 1870° C for 1 hour.

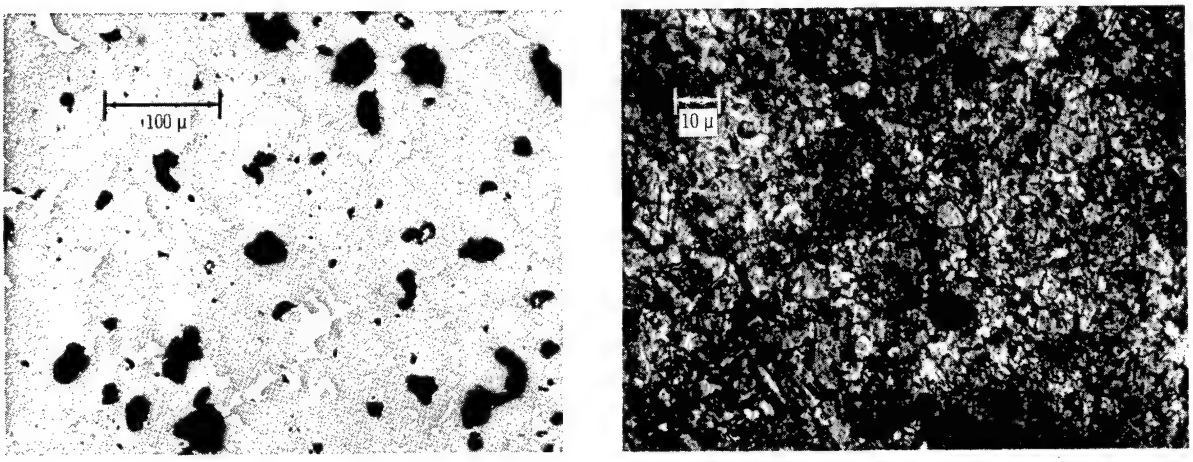

(a) Unetched. (b) Etchant, hydrofluoric acid.

Figure 21. - Microstructure of zirconia with 15 mole percent titanium, cold-pressed, and sintered in vacuum at 1870° C for 1 hour.

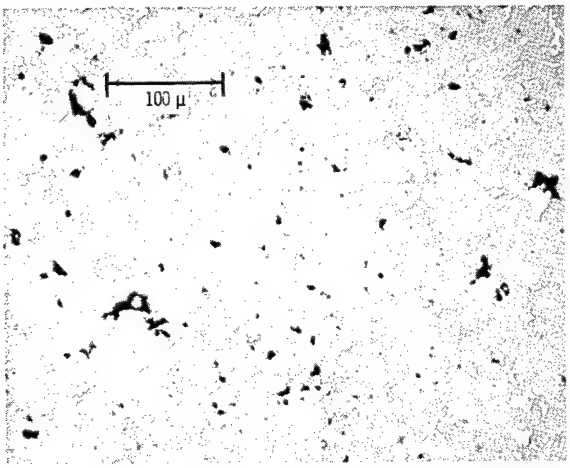

Figure 22. - Microstructure of zirconia with 15 mole percent titanium, hot-pressed in vacuum at 1600° C and 2000 psi for 1 hour. Unetched.

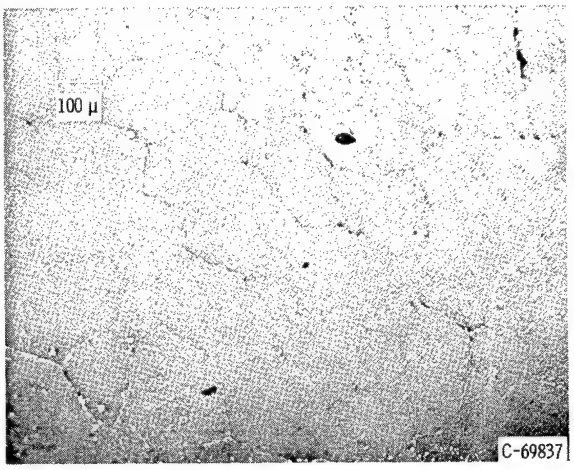

Figure 23. - Microstructure of pure zirconia after vacuum hot-pressing at 2025° C and 2000 psi for 1 hour. Unetched.

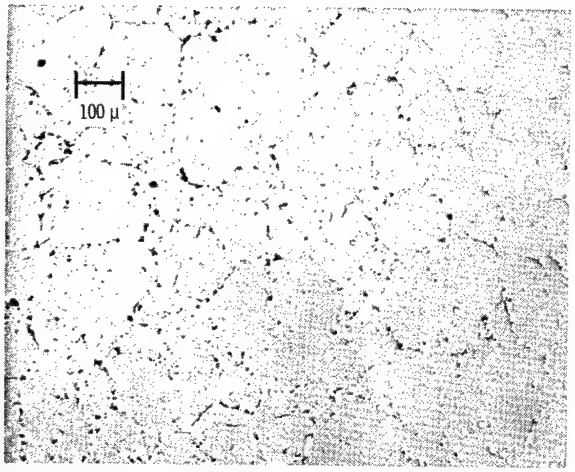

Figure 24. - Microstructure of zirconia with 15 mole percent zirconium, milled, cold-pressed, and sintered in vacuum at 1870° C for 1 hour. Unetched.

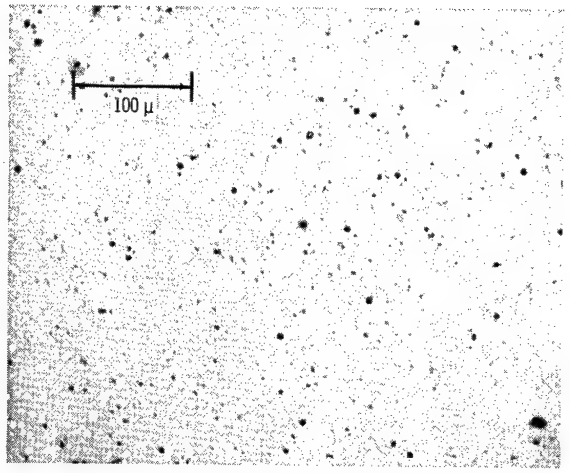

Figure 25. - Microstructure of zirconia with 15 mole percent chromium, milled, cold-pressed, and sintered in vacuum at 1870° C for 1 hour. Unetched.

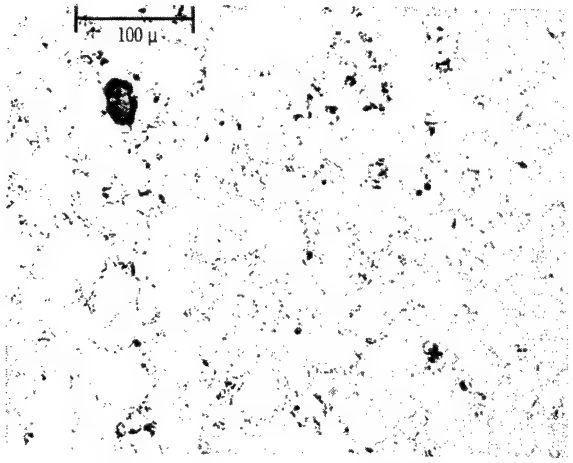

Figure 26. - Microstructure of zirconia with 15 mole percent vanadium, milled, cold-pressed, and sintered in vacuum at 1870° C for 1 hour. Unetched.

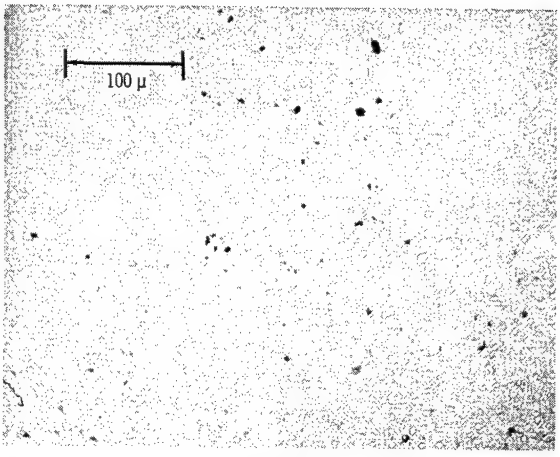

Figure 27. - Microstructure of hafnia with 15 mole percent titanium, milled, cold-pressed, and sintered in vacuum at 1870° C for 1 hour. Unetched.

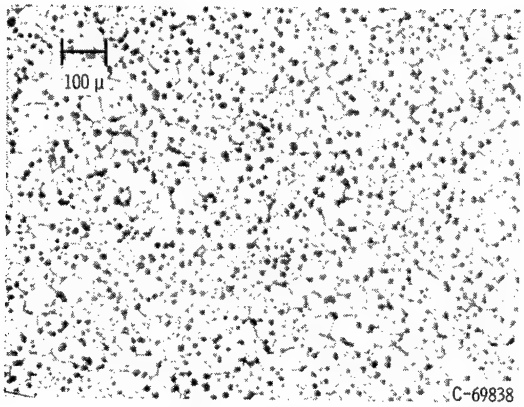

Figure 28. - Microstructure of calcia-stabilized zirconia (Zircoa B), milled, cold-pressed, and sintered in air at 1800° C for 3 hours. Etchant, fused potassium bisulfate.

investigation are shown in figures 20 to 28. Of these, only figures 20 to 22 are for the various zirconia-titanium compositions already discussed. The other figures are for zirconia with other metal additions, but these will be discussed later.

Comparison of figures 20 and 21 shows the effects of milling on porosity, grain size, and dispersion of the metallic phase. Comparison of figures 20 (or 21) and 28 shows the rather large difference in grain size between the zirconia-titanium compositions and calcia-stabilized zirconia for similar heat treatments.

Density. - The densities of the compositions used in this investigation are given in table II.

Heat capacity. - Figure 29 shows ΔH and c_p as functions of temperature for the milled zirconia with 15 mole percent titanium (ZT-15-M) only. The results agree fairly well with those given in the literature for pure zirconia (ref. 18). The discrepancies in the results are within the limits of experimental error (approx. 5 percent in the present investigation). The corrections to be applied for the heat-capacity difference between titanium and zirconia or for the heat of transformation of titanium do not change these results significantly.

Thermal conductivity and thermal diffusivity. - Figure 30 shows the thermal conductivity k as a function of temperature for ZT-15-M (see table II). The thermal conductivity of calcia-stabilized zirconia (ref. 26) is plotted in the same figure for comparison purposes. As shown, the thermal conductivity of ZT-15-M is consistently higher than that of calcia-stabilized zirconia. The reason for this discrepancy can be explained through the following analysis.

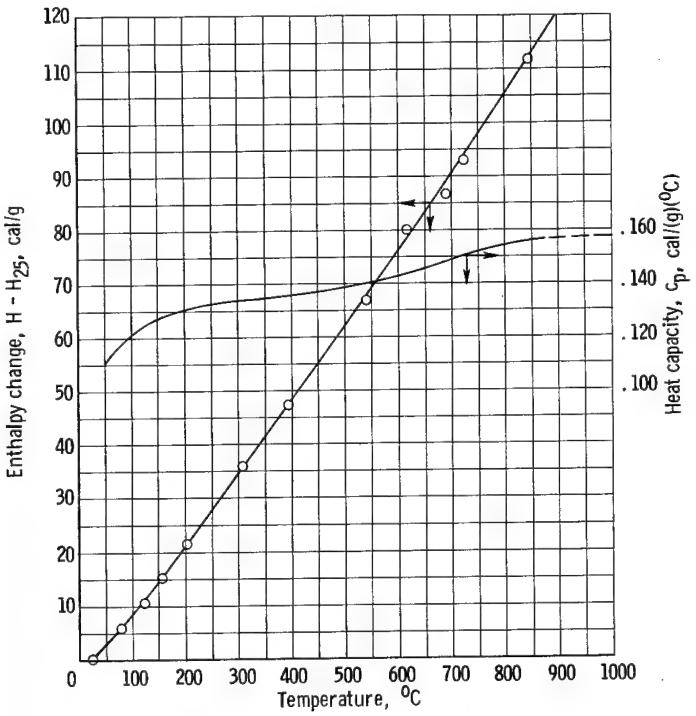

Figure 29. - Enthalpy and heat capacity of zirconium oxide with 15 mole percent titanium (ZT-15-M) as function of temperature.

On the assumption that the thermal conductivity of the continuous phase in the zirconia-titanium composition is the same as that of stabilized zirconia, the thermal conductivity of a structure like that shown in figure 20 can be calculated (ref. 26) to be

$$k_m = k_c \frac{1 + 2V_d \dfrac{1 - \dfrac{k_c}{k_d}}{2\dfrac{k_c}{k_d} + 1}}{1 - V_d \dfrac{1 - \dfrac{k_c}{k_d}}{\dfrac{k_c}{k_d} + 1}} = 0.0055 \frac{(cal)(cm)}{(cm^2)(sec)(^oC)} \qquad (6)$$

where

k_m thermal conductivity of mixture

k_c thermal conductivity of continuous phase (at room temperature), $\cong$ 0.0047

V_d fractional volume of dispersed phase, $\cong$ 0.082

k_d thermal conductivity of dispersed phase (at room temperature), $\cong$ 0.044

If the metallic phase had been assumed to be in the form of slabs parallel to the direction of heat flow, the calculated thermal conductivity would have been (ref. 26)

$$k_m = V_d k_d + (1 - V_d)k_c = 0.0079 \quad \frac{(cal)(cm)}{(cm^2)(sec)(^oC)} \qquad (7)$$

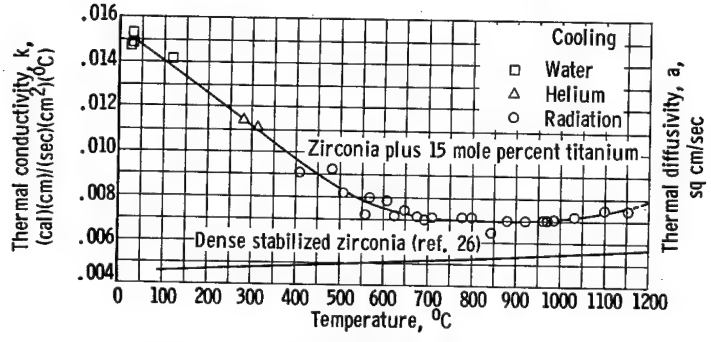

Figure 30. - Thermal conductivity of zirconium oxide with 15 mole percent titanium (ZT-15-M) as a function of temperature compared with that of stabilized zirconia (ref. 26).

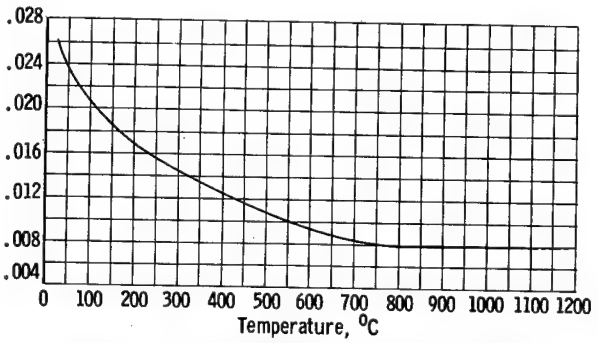

Figure 31. - Thermal diffusivity of zirconium oxide with 15 mole percent titanium (ZT-15-M).

The experimentally determined thermal conductivity at room temperature (fig. 30) was 0.015 calorie per centimeter per second per °C. It is concluded from these values that the larger thermal conductivity of the zirconia-titanium composition is due mainly to the larger thermal conductivity of monoclinic zirconia compared with that of the cubic calcia-stabilized zirconia.

The thermal diffusivity a as a function of temperature for ZT-15-M (fig. 31) calculated by using the heat capacity from figure 29 and the density ρ (5.70 g/cc, from table II) through the defining equation (5)).

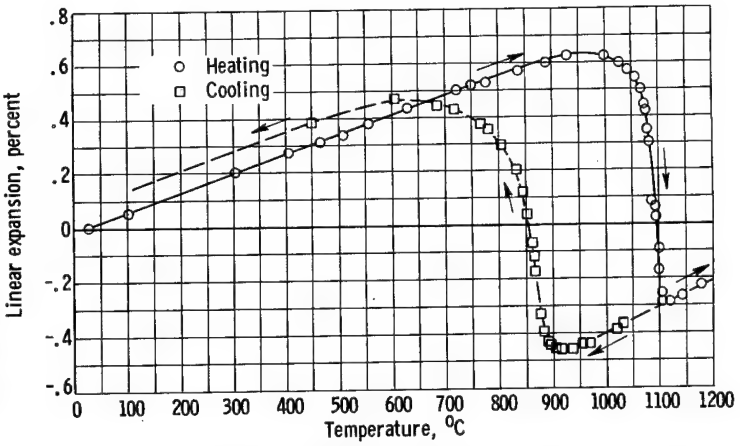

Figure 32. - Linear thermal expansion of zirconium oxide with 15 mole percent titanium (ZT-15-M).

Thermal expansion. - Figure 32 shows the thermal expansion of the milled, cold-pressed, and sintered composition of zirconia with 15 mole percent titanium (ZT-15-M) as a function of temperature. The transformation temperatures, both on heating and cooling, as well as the shape of the thermal-expansion - temperature curves are essentially the same as those given in reference 22. The actual expansion through the transition temperature was 0.92 percent against approximately 0.47 percent reported in reference 22. In the present investigation, the α between 25° and 900 °C was 7.05×10^{-6} °C against 7.65×10^{-6}° C (ref. 22). In either case, the value of α for the zirconia-titanium composition is lower than the value of 10.0×10^{6} °C reported in the literature for calcia-stabilized zirconia (ref. 26). It was also noted in the present investigation that expansion through the transformation range could be arrested by holding the temperature constant even in the regions of maximum slope α.

The discrepancies between the coefficients of thermal expansion of the zirconia-titanium compositions reported in the literature and those found in this investigation may be due to differences between the reported and actual thermal expansions of the tungsten standard used in the present investigation (see appendix D), the anisotropy of the samples, or to differences in composition. It will be shown later that anisotropy could be produced by stresses induced by heating or cooling.

Modulus of rupture. - For four-point loading, the number of specimens was too small to determine the effects of beam height, width, and distance between the points of load application on the modulus of rupture. Taken together, however, the average of the values under four-point loading and under three-point loading at room temperature were found to differ significantly. The average of 24 values under four-point loading was 32,400 psi against an average of eight specimens of 42,900 psi on three-point loading, all at room temperature. This gave a ratio of room temperature modulus-of-rupture values of 0.76. Then, from equation (3),

$$\sigma_{M_T,2} = 0.76\ \sigma_{M_T,1} \tag{8}$$

The modulus of rupture $\sigma_{M_T,2}$ as a function of temperature for zirconia with 15 mole percent titanium, milled, cold-pressed, and sintered (ZT-15-M), is shown in figure 33. The modulus of rupture for cold-pressed and sintered zirconia with 15 mole percent titanium (ZT-15) as a function of temperature is shown in figure 34. Figure 35 shows the modulus of rupture of milled and sintered calcia-stabilized zirconia (BM) as a function of temperature.

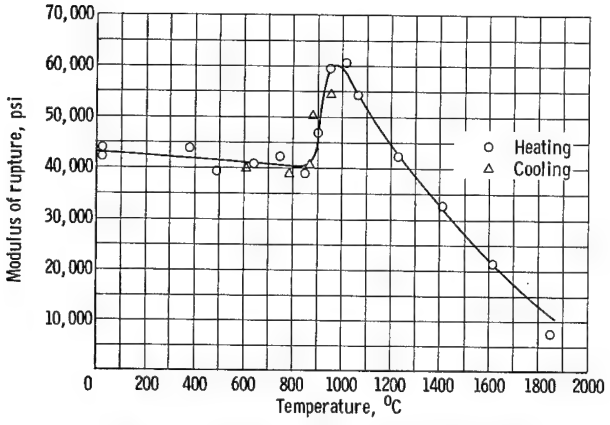

Figure 33. - Modulus of rupture under three-point loading for zirconium oxide with 15 mole percent titanium (ZT-15-M) as function of temperature.

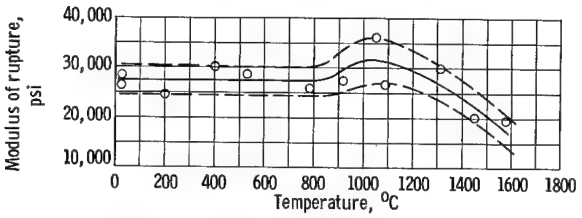

Figure 34. - Modulus of rupture under three-point loading for zirconia with 15 mole percent titanium (ZT-15) as function of temperature (heating cycle only).

As shown in figure 33, there is a maximum in the curve for modulus of rupture against temperature at about 950° C. The same maximum is suggested in the curve shown in figure 34 for the cold-pressed and sintered material (ZT-15), but this maximum is not very definite because of the large scatter in the modulus-of-rupture values. This scatter is attributed to the porosity of the compositions. The larger modulus of rupture of the milled zirconia-titanium compositions compared with the same type of material without milling is ascribed to the smaller porosity and grain size of the milled compositions (figs. 20 and 21, p. 21). The maximum in these curves is attributed to the higher strength of the tetragonal phase.

Comparison of figures 34 and 35 shows that the modulus of rupture of the zirconia with 15 mole percent titanium composition is almost twice that of stabilized zirconia at low temperatures for equivalent porosity (figs. 21 and 28, pp. 21 and 22). At high temperatures, the modulus of rupture of the zirconia-titanium compositions is definitely superior to that of stabilized zirconia. For example, at 1200° C, the modulus of rupture at ZT-15 is 30,000 psi against about 2000 psi for calcia-stabilized zirconia. The reason for this could be the inherent strength of tetragonal zirconia or the strengthening effect of the metal (i.e., by relieving stress concentrations). Although at high temperatures the strength of the zirconia-titanium compositions is definietly superior to that of stabilized zirconia, the low-temperature superiority in strength probably reflects grain size effects in addition to inherent material differences.

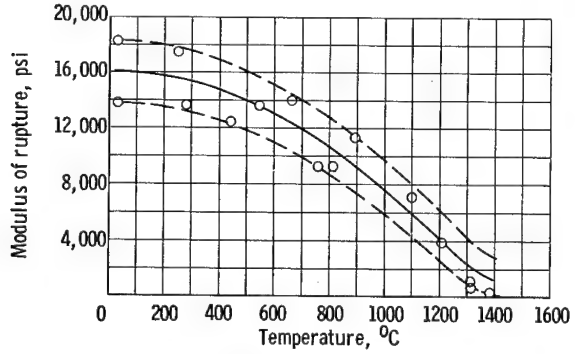

Figure 35. - Modulus of rupture under three-point loading for 5 weight percent calcia-stabilized zirconia as function of temperature (heating cycle only).

The effects of grain size on strength can be calculated from Knudsen's equation (ref. 27). Unfortunately, the material constants for zirconia to be used in this equation are not known, but experimental data on materials like alumina and magnesia (ref. 28) indicate that a ratio of 1/10 grain sizes would give a

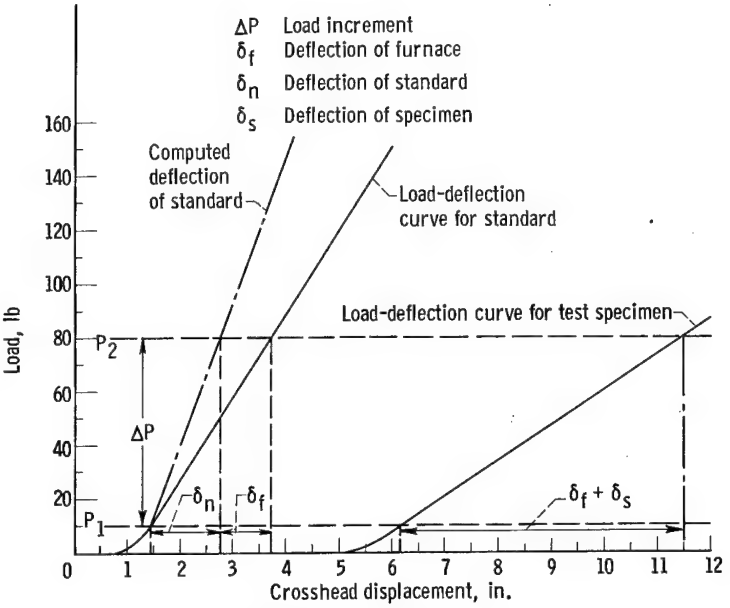

Figure 36. - Load-deflection curves for modulus-of-elasticity specimen and standard at room temperature (schematic). (These are not actual load-deflection curves but idealized curves illustrating meaning of symbols used in appendix F.)

strength ratio of about 2. As shown in figures 21 and 28, the ratio of the grain size of ZT-15 to that of stabilized zirconia is just about 1/10. From this, it is concluded that the increase in low-temperature strength of zirconia by additions of titanium is due, in part, to the smaller grain size of the zirconia-titanium compositions.

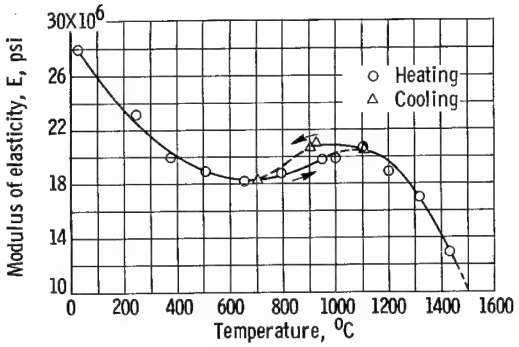

Figure 37. - Modulus of elasticity of zirconium oxide with 15 mole percent titanium (ZT-15-M) as function of temperature.

Modulus of elasticity. - The static modulus of elasticity of milled zirconia with 15 mole percent titanium (ZT-15-M) was measured as a function of temperature by using the equipment and method described in appendix F. Schematic load-deflection curves for specimen and standard illustrating the meaning of the symbols used in appendix F are shown in figure 36. The static modulus of elasticity E as a function of temperature for milled, cold-pressed, and sintered zirconia with 15 mole percent titanium (ZT-15-M, table II) obtained by the bending method is shown in figure 37. The dynamic modulus of elasticity at room temperature was 29.6×10^6 psi compared with 28.0×10^6 psi for the static modulus by bending. The room temperature compressive load-deflection curves are shown in figure 38. The modulus of elasticity in compression was 28.2×10^6 psi and Poisson's ratio was 0.242. The static moduli of elasticity of zirconia with 15 mole percent titanium (ZT-15-M) - both in tension and compres-

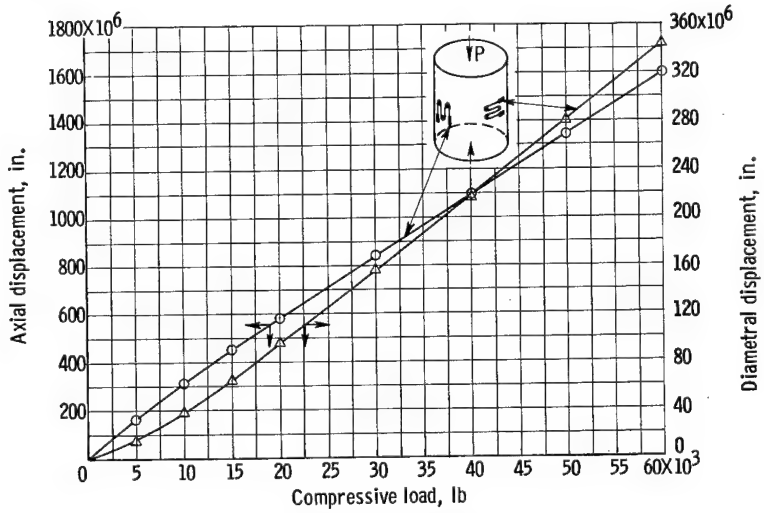

Figure 38. - Curves for compression load against strain for zirconium oxide with 15 mole percent titanium (ZT-15-M) at room temperature. Bridge, BLH SR-4; strain gages: Budd Co. Type C-12; specimen diameter, 1.326 in.; modulus of elasticity 28.2×10^6 psi; Poisson's ratio, 0.242.

sion - are, for all practical purposes, identical, and the modulus of rupture needs no correction. The static modulus of elasticity in tension for the zirconia-titanium compositions (ZT-15-M) is larger than the reported value for 5 weight percent calcia-stabilized zirconia. A value of 20.45×10^6 psi at room temperature was reported for 5 weight percent calcia-stabilized zirconia with a density of 4.93 grams per cubic centimeter (ref. 29). Although the curve for modulus of elasticity against temperature for 5 weight percent calcia-stabilized zirconia (ref. 29) tends to flatten out at about 700° C, it does not have the hump shown by the curves for zirconia-titanium material at about 1000° C (fig. 37). The discrepancy in the values of E of ZT-15-M (see table II) and calcia-stabilized zirconia may be due, in part, to the low density of the stabilized zirconia. The effects of grain size on E appear to be negligible (ref. 28).

Some of the bars of ZT-15-M used for the determination of E as a function of temperature have a slight curvature after a series of runs. It was thought at the time of the experiments that this curvature was associated with the low-temperature creep and plasticity reported in reference 9 for similar zirconia-titanium compositions. Experiments to be described later on in this report will clarify this point.

Comparison of Calculated and Experimental Thermal Shock Resistance

Theoretical considerations. - In this investigation, the thermal shock resistance of zirconia with metal additions is determined by quenching disks with thermally insulated faces. This method of determining thermal shock resistance was originally used by the investigators of reference 10 for determining the thermal shock resistance of steatite disks and is amenable to mathematical treatment; that is, the thermal shock parameter ΔT can be correlated with the physical properties of the material. The mathematical treatment for the case of a thin disk is similar to that for an infinite cylinder developed in reference 15.

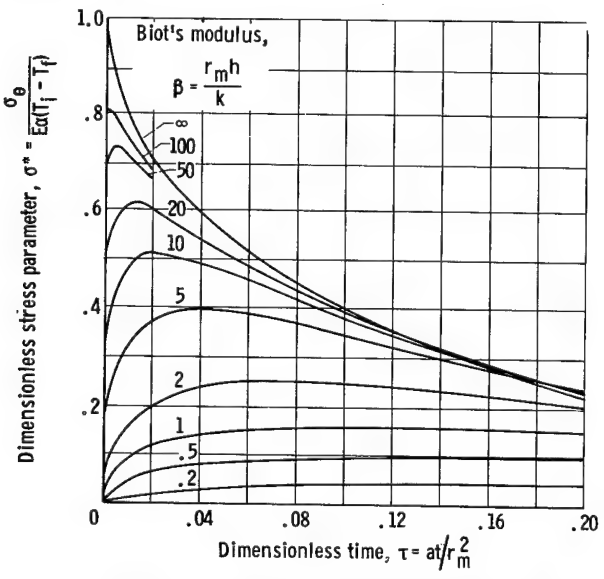

Figure 39. - Dimensionless stress against dimensionless time for several values of Biot's modulus (ref. 10).

The results of reference 15 were modified in reference 10 to obtain an expression for the relation between the tangential surface stress, time, and heat-transfer coefficient during the transient heating or cooling of a disk with thermally insulated faces. This relation is shown in terms of dimensionless variables in figure 39 (taken from ref. 10) where σ^* is the dimensionless stress parameter, τ is dimensionless time, β is Biot's modulus, t is the time from the start of cooling, r_m is the maximum radius of the disk, T_i is the initial (uniform) temperature of the disk, T_f is the final (uniform) temperature of the disk (temperature of quenching medium), σ_θ is the tangential stress at the

periphery of the disk at time t, E is Young's modulus of elasticity, and α is the coefficient of linear thermal expansion.

For quenches from below the transformation temperature, specimens crack when the tangential stress at the periphery of the disk equals the strength of the material. For any given value of Biot's modulus β, the dimensionless rupture stress σ^* or the corresponding maximum tangential stress $\sigma_{\theta_{max}}$ is that corresponding to the maximums in the σ^* against τ curves. Since for every β there is a maximum in the corresponding curve, the maximum dimensionless stress can be represented as a function of β by

$$\sigma^*_{max} = \frac{\sigma_{\theta_{max}}}{E\alpha(T_i - T_f)} = \frac{1}{f(\beta)} \tag{9}$$

where $f(\beta)$ is to be determined by curve fitting. From equation (9) it follows that

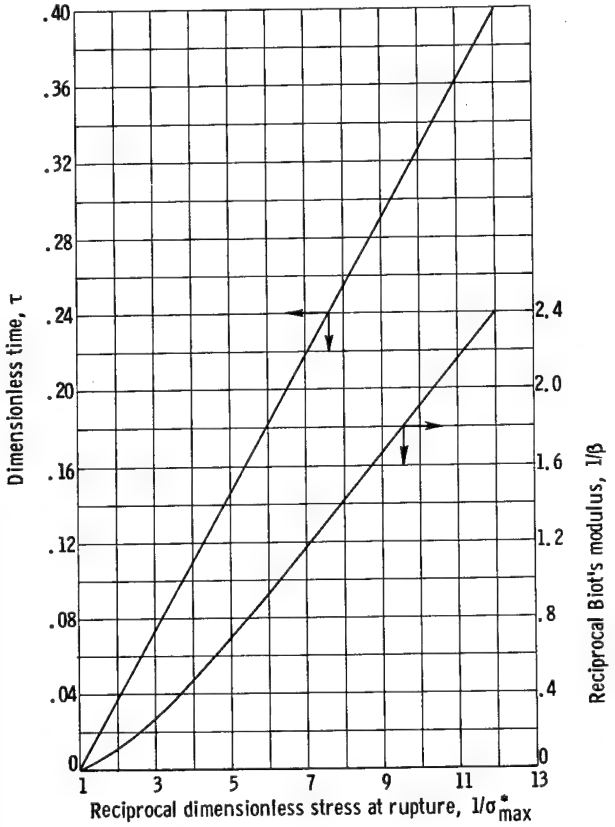

Figure 40. - Plots of dimensionless time against reciprocal dimensionless stress at rupture and reciprocal Biot's modulus against reciprocal dimensionless stress at rupture for a thin disk.

$$\Delta T = T_i - T_f = \frac{\sigma_{\theta_{max}}}{E\alpha} \times f(\beta) \tag{10}$$

The values of $1/\beta$ against $1/\sigma^*_{max}$ have been plotted in figure 40 from the data in figure 39. For the range above $1/\beta \cong 0.4$, $f(\beta)$ was calculated as (ref. 12)

$$f(\beta) = 2 + \frac{4.3}{\beta} = 2 + 4.3\,\frac{k}{hr_m} \tag{11}$$

whence

$$\Delta T = \frac{\sigma_{\theta_{max}}}{E\alpha}\left(2 + 4.3\,\frac{k}{hr_m}\right) \tag{12}$$

Equations (10) and (12) are the thermal shock equations for a thin disk. These equations were derived on the assumption of temperature independent σ_θ, E, α, and k. As a general rule, these properties are functions of T, and, in this case, the values to be used in either of the thermal shock equations are, to a first approximation, those corresponding to the temperature at $r = r_m$ at the moment of rupture.

The time at the moment of rupture can be determined from figure 39, since rupture occurs at the τ corresponding to the maximums in the curves. The

plot of τ against $1/\sigma_{max}$ is shown in figure 40. The corresponding values of τ as a function of β or $1/\beta$ can be obtained from the same figure. Thus, if the surface heat-transfer coefficient h is known, the time at rupture can be determined. If, in addition, cooling curves such as those shown in figure 5 (p. 12) are available, the temperature at rupture at some specific point in the specimen can be determined. In this investigation, the principal concern is with values of the temperatures mainly at the surface or at the center of the disk. The cooling curve at the center is easily obtained by a thermocouple at this point, but the surface-cooling curve must be obtained by extrapolation or by calculation because of the experimental difficulty of locating a thermocouple at the periphery of the disk. Then, if the properties in the thermal shock equations are known as a function of temperature, ΔT as a function of assumed values of hr_m can be determined. This ΔT is usually taken as a measure of relative thermal shock resistance, and plots of ΔT against hr_m allow the selection of materials on the basis of their thermal shock resistance under the actual heat-transfer coefficient where they are to be used (refs. 11 and 12). The values of ΔT obtained by substitution of the properties in the thermal shock equation (eq. (12)) will be termed the calculated thermal shock resistance, as distinguished from that obtained by quenching experiments, which will be termed the experimental thermal shock resistance.

In the present investigation, the preceding theory applies only to specimens quenched from below the transformation temperature range. On quenches through the transformation temperature, the surface is in compression and the center is in tension at the moment of rupture, because α is negative through the transformation range. Since the compressive strengths of ceramics are several times larger than the tensile strengths (refs. 4 and 26), the specimens fail in tension at the center on cooling through the transformation range. From the equations for the stresses in a thin disk during heating or cooling given in reference 17, it can be shown that, if E and α are assumed constant and, as is the case in the present investigation, the temperature distribution in the disk is parabolic, the numerical value of the stress at the center is about one-half that of the stress at the rim of the disk but opposite in sign. Consequently, ΔT for quenches through the transformation range is twice that given by equation (10) or (12). A look at the thermal-expansion - temperature curve for the zirconia-titanium compositions under consideration (ref. 22)[1] will show that, because of the very large negative values of α on cooling through the transformation range, if the disk is to crack under the given h with the testing method used in this investigation, rupture will occur when the center reaches the temperature corresponding to the start of the transformation, because it is at this point that the tensile stresses at the center are a maximum.

The validity of using the thermal shock equation for a material undergoing an allotropic transformation is subject to question; however, in this investigation, the equation will be used for comparing calculated and experimental thermal shock resistances. Because of the possible formation of stress-raising

[1]The curve in reference 22 is almost identical with that shown in figure 32 in this report.

cracks during the transformation, it can be surmised that if the material behaves elastically and the other properties entering into the thermal shock equation are substantially constant, the only effect of the cracks would be to make the experimental thermal shock resistance lower than the calculated thermal shock resistance.

The stress gradient (partial derivative of σ with respect to r in eq. (3)) at the center of the disk is zero and consequently for the calculated thermal shock resistance on quenching through the transformation range of zirconia-titanium compositions, the tensile strength rather than the modulus of rupture of the material is to be used in the thermal shock equation. As is customarily done for brittle materials, the tensile strength will be assumed to be one-half the modulus of rupture (ref. 30). This new factor of one-half cancels the factor two obtained in the previous argument, and the thermal shock equations (10) and (12) apply equally well for quenches both from below and through the transformation range, provided that the modulus of rupture $\sigma_{M_{T,2}}$ is used for $\sigma_{\theta_{max}}$. For the reasons already stated, this value of modulus of rupture - as well as all the other properties in the thermal shock equation - is that at the temperature corresponding to the start of the transformation.

Procedure for calculating thermal shock resistance from material properties. - In this procedure for calculating the curve for ΔT against hr_m, the properties to be used in the thermal shock equations (eqs. (10) and (12)) are those obtained at the time and position at which rupture occurs. Two distinct cases will be considered: quenches from below the transformation range and quenches through the transformation range.

For quenches from below the transformation range it is convenient to restate the thermal shock equation (eq. (10)) in a different form. From the definition of relative temperature at $r = r_m$,

$$U_{1.0} = \frac{T_s - T_f}{T_i - T_f} = \frac{T_s - T_f}{\Delta T} \tag{13}$$

where T_s is the temperature at $r = r_m$ and time t from the start of cooling. Substituting ΔT from equation (13) into equation (10) and rearranging terms yield

$$U_{1.0} f(\beta) = \frac{E\alpha}{\sigma_{\theta_{max}}} (T_s - T_f) \tag{14}$$

Substituting the modulus of rupture $\sigma_{M_{T,2}}$ from equation (8) for the maximum tangential stress $\sigma_{\theta_{max}}$ in equation (14) gives

$$U_{1.0} f(\beta) = \frac{E\alpha}{0.76\ \sigma_{M_{T,1}}} (T_s - T_f) \tag{15}$$

At the moment of rupture, E, α, and $\sigma_{M_{T,1}}$ are taken as the properties at T_s.

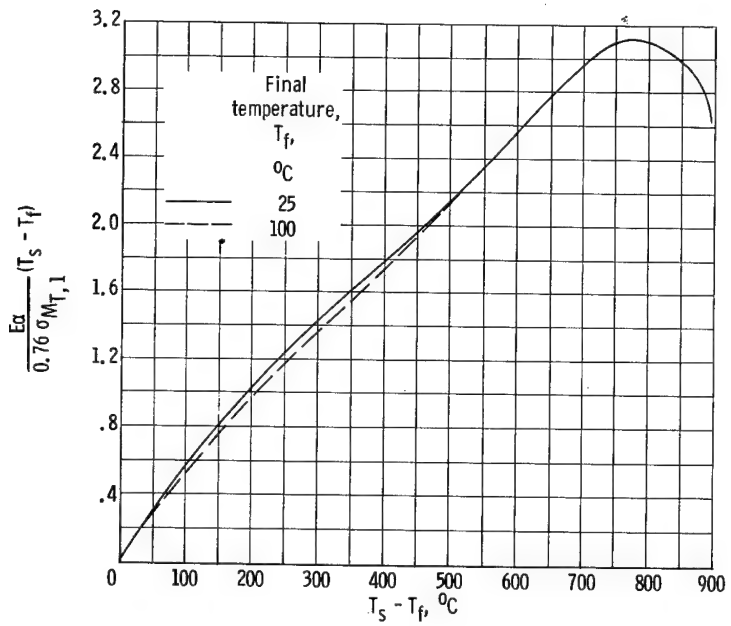

Figure 41. - Variation of $\frac{E\alpha}{0.76\,\sigma_{M_{T,1}}}(T_s - T_f)$ as function of $T_s - T_f$.

In order to facilitate computations, it is advantageous to plot the right side of equation (15) as a function of $T_s - T_f$. This plot is shown in figure 41 for two different values of T_f.

Plots of β as a function of $U_{1.0}$ and of τ are also required. These plots are shown in figure 42. The data for these plots were obtained from Russell's tables (ref. 14).

The procedure used to obtain the points to plot the curve for ΔT against hr_m for quenches from below the transformation range is illustrated with an example as follows:

(1) A value of Biot's modulus $\beta = 8.2$ was assumed. From figure 40, $f(\beta) = 2.10$ and $\tau = 0.04$.

(2) From the pair of values from step (1) (β,τ) and figure 42, $U_{1.0} = 0.275$.

(3) From the product of the values of $f(\beta)$ and $U_{1.0}$ from steps (1) and (2) and from figure 41, $T_s - T_f = 104^\circ$ C and $T_s = 129^\circ$ C.

(4) From the value of $T_s - T_f$ from step (3) and equation (13), $\Delta T = 378^\circ$ C.

(5) From figure 30 (p. 24) and $T_s = 129^\circ$ C from step (3), $k = 0.0136$.

(6) From the value of assumed β, $k = 0.0136$ from step (5), and the defining equation for β (see fig. 39, p. 28 or appendix A), $hr_m = 0.112$.

(7) The value of ΔT from step (4) and hr_m from step (6) gave a point on the curve. Similarly, other points were plotted to obtain the whole curve.

For the reasons already stated, the calculated ΔT for quenches through the transformation range were obtained from the values of the properties at 880° C (region of maximum α).

Comparison of experimental and calculated thermal shock resistance of zirconia with 15 mole percent titanium. - The values of ΔT and hr_m obtained by the procedure described in the previous section were plotted as shown in figure 16 (p. 19). Comparison with the experimental thermal shock resistance in the same figure shows that, for quenches from below the transformation range

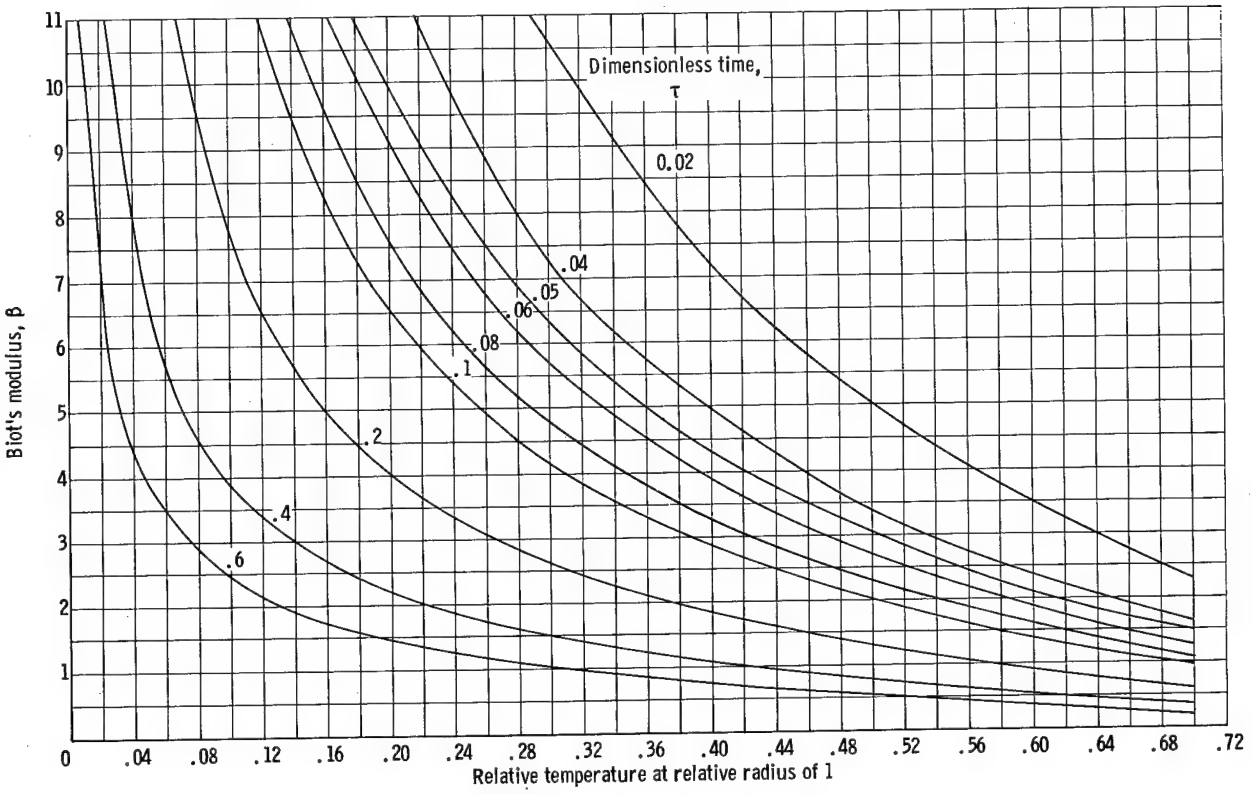

Figure 42. - Plot of Biot's modulus against relative temperature at relative radius of 1.

of ZT-15-M (see table II), the thermal shock resistances obtained from theory and experiment are, for all practical purposes, identical. For quenches through the transformation range, on the other hand, the experimental thermal shock resistance is about seven times the calculated value. In this latter case, the discrepancy between calculated and experimental values is too large to be attributable to experimental errors or to the approximations used in the calculations, and the discrepancy must be ascribed to other causes. As stated in the INTRODUCTION, the investigation of these causes will be the subject of a separate section in this report.

Effect of grain size on thermal shock resistance. - Introducing the effects of grain size and porosity into the thermal shock equation (eq. (12)) by means of Knudsen's equations (ref. 27) for E and $\sigma_{\theta_{max}}$ and an equation for the effects of porosity on thermal conductivity (ref. 26) yields

$$\Delta T = \frac{\sigma_0 G^{-A}}{\alpha E_0}\left[2 + 4.3\,\frac{k_0}{hr_m}\,(1 - P)\right] e^{-(B-C)P} \qquad (16)$$

where A, B, C, and σ_0 are material constants, G is the grain size in microns, and P is the fractional porosity. The symbols E_0, $\sigma_0 G^{-A}$, and k_0 can be regarded as Young's modulus, modulus of rupture, and thermal conduc-

tivity, respectively, at zero porosity. Equation (16) can be used for comparing the thermal shock resistance of different materials if the constants in the equation, the fractional porosities, and the grain sizes for the materials in question are known. Unfortunately, the constants in equation (16) are not available for zirconia, but published data (ref. 28) for alumina and magnesia show that the constants A, B, and C are nearly the same for both materials ($A \cong 1/3$). To a first approximation, it can be assumed that the same would be true for materials like zirconia-titanium and calcia-stabilized zirconia. From these considerations it can be surmised that the greater thermal shock resistance of ZT-15 compared with that of calcia-stabilized zirconia (see fig. 18, p. 19) is due, in part, to the smaller grain size of the former (see figs. 21 and 28, pp. 21 and 22). Since grain size affects strength without appreciably affecting modulus of elasticity, coefficient of thermal expansion, or thermal conductivity, it can be surmised that smaller grain size increases thermal shock resistance by increasing the modulus of rupture.

Elucidation of Mechanism by Which Titanium Improves Thermal Shock Resistance of Zirconia

General considerations. - As already stated, the good thermal shock resistance of the zirconia-titanium compositions for quenches from below their transformation range can be explained on the basis of the smaller grain size - and hence higher strength - of these compositions compared with that of the calcia-stabilized zirconia. This grain size difference may be due to inherent properties of the matrix materials, to the effect of calcia on the grain growth of zirconia, or to the effect of titanium in inhibiting the grain growth of zirconia. For this reason, experiments to determine the effect of titanium on grain growth were carried out.

On the other hand, it has been shown in a previous section that the discrepancy between the experimental and calculated thermal shock resistance of milled zirconia with 15 mole percent titanium for quenches through its transformation range cannot be explained solely from the values of the material properties that appear in the thermal shock equation alone, and some other explanation must be sought. As already mentioned, zirconia-titanium disks cracked by thermally shocking them through the transformation range have open cracks (fig. 19, p. 20), and during the determination of the modulus of elasticity, some of the test bars came out of the furnace with a slight curvature. It was reported in reference 9 that zirconia with 15 mole percent titanium compositions exhibited plasticity at room temperature at stress levels as low as 15,000 psi (maximum fiber stress), but no evidence of such behavior was noted in room-temperature modulus of elasticity and modulus-of-rupture determinations for the zirconia-titanium compositions tested in this investigation. For this reason, experiments were conducted to determine the lowest temperature at which plastic deformation could be observed in the zirconia-titanium material used in this investigation.

Effects of titanium additions on grain growth of zirconia. - Small specimens of pure zirconia (CP Zirox, table I) were cold-pressed and vacuum-sintered by the same techniques used for the ZT-15 zirconia-titanium composition. The microstructure of the vacuum-sintered pure zirconia is shown in figure 43(a) and that of the ZT-15 composition in figure 21. The black and

dark gray areas in figure 43(a) and the black areas in the unetched photomicrograph in figure 21 (p. 21) are voids. Comparison of these figures shows that despite the fact that pure zirconia was sintered at a slightly lower temperature its grain size is about five times that of the zirconia with the titanium addition. It is concluded from this experiment that the titanium additions inhibit the grain growth of zirconia and thereby increase its strength.

Elastoplastic phenomena on heating and cooling through transformation range. - In an attempt to determine the temperature at which the modulus-of-elasticity specimens bent, additional experiments were carried out. The modulus-of-rupture tester shown in figure 12 (p. 17) was modified to accommodate specimens 2.35 inches long by 0.50 inch wide by 0.100 to 0.125 inch high. (The specimens could be positioned under the push rod for loading or removed from the loading position at any time, as explained in reference 13.

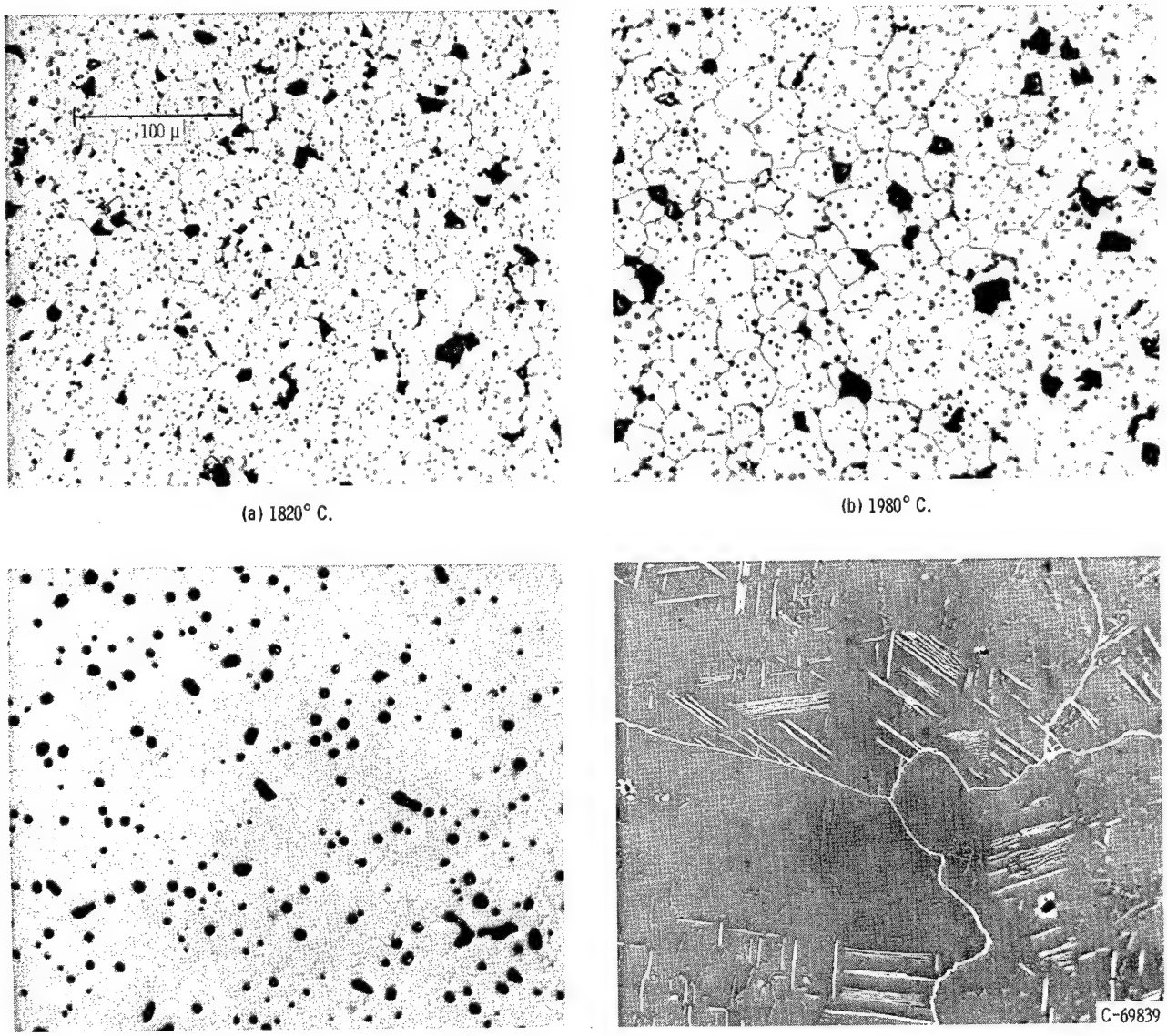

(a) 1820° C.

(b) 1980° C.

(c) 2400° C.

(d) 2620° C.

Figure 43. - Microstructures of pure zirconia after vacuum sintering for 1 hour at various temperatures. Unetched. X250.

The specimen was heated at a rate between 3° and 5° C per minute (in vacuum) under a constant stress of about 50 percent of its rupture stress. Constant recordings of the deflections at this constant stress were taken. Under these conditions, the recorded deflection was the specimen deflection plus the (thermal) expansion of the furnace. The furnace expansion as a function of temperature was determined in a separate run under the same conditions used in the test, except that a thick tungsten specimen was used instead of the zirconia-titanium specimen. The zirconia-titanium specimen deflection was obtained by subtracting the furnace expansion from the recorded deflection with the specimen.

The same procedure was used with a different specimen for determining deflections on cooling except that the specimen was heated above the transformation range without load before cooling under load.

Deflections for the heating and cooling cycles for type ZT-15-M composition (table II) are shown in figure 44 together with a curve for thermal ex-

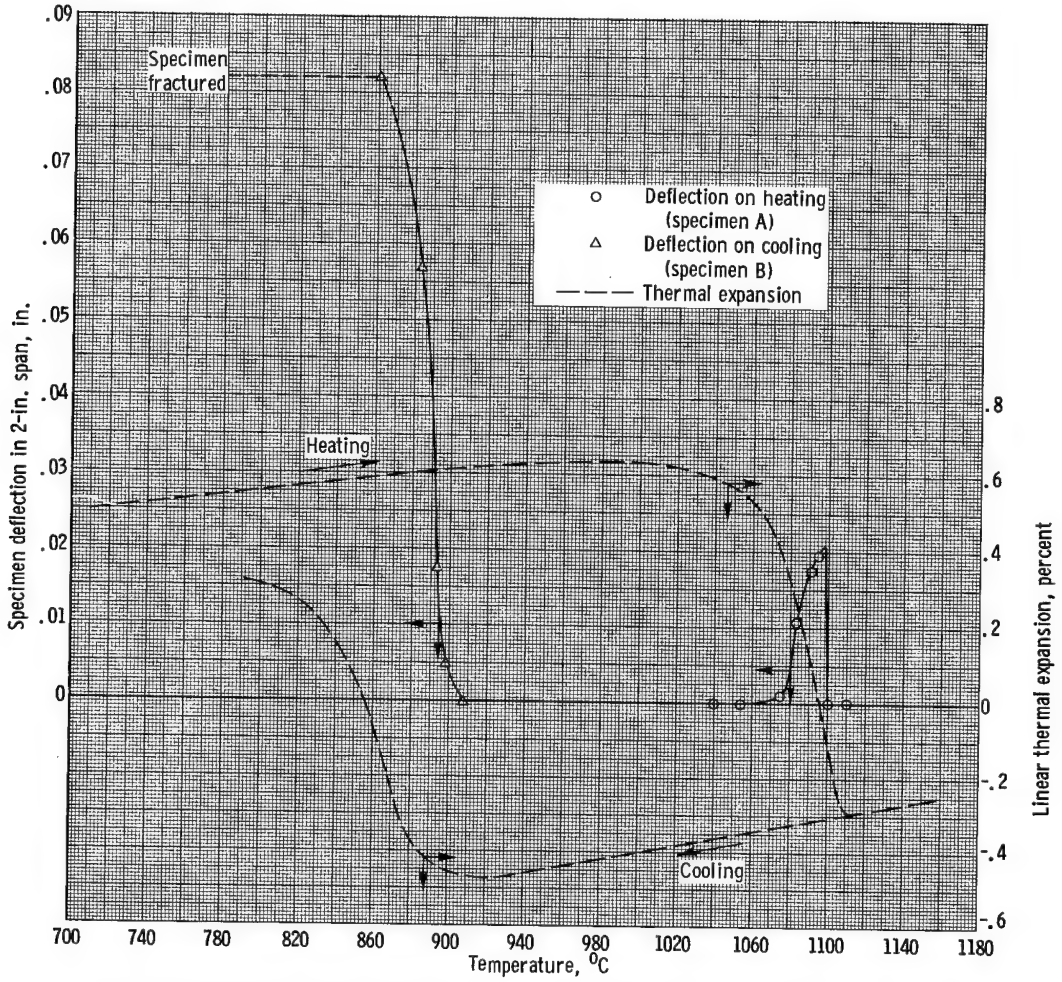

Figure 44. - Plastic deformation of zirconium oxide with 15 mole percent titanium (ZT-15-M) on heating and cooling through transformation range showing correspondence with thermal expansion curves. Specimen dimensions, 0.500 inch wide by 0.100 inch thick; maximum fiber stress, 21,000 psi; heating rate, 3.7° C per minute; cooling rate, 4.5° C per minute.

pansion against temperature for the same material.

On heating the zirconia-titanium composition (ZT-15-M) at temperatures below its transformation range (~1000° to 1100° C) under 50 percent of maximum load (i.e., approx. 22,000 psi maximum fiber stress) no measurable specimen deflection was noted. On heating through the transformation range under the same loading conditions, the material deformed plastically up to near the maximum in the deflection-temperature curve. At this point the specimen deformed faster than the speed of the tensile machine at that moment (the deformation was too fast to follow with the low-speed range of 0.200 in./min, maximum, being used at the time), so that actually the specimen was deforming under zero external load. About 10 seconds later, the tensile machine showed a very rapid increase in load, and the crosshead motion had to be reversed rapidly in order to prevent breaking the specimen. In about 30 seconds, the specimen straightened itself out and retained this flat shape to at least 50° C above the transformation range. On cooling this same specimen through the transformation range without load, the specimen acquired the same maximum curvature it had just before straightening out and retained this curvature on cooling to room temperature.

In order to study the behavior in the cooling cycle, a new, originally flat specimen was heated under zero load (actually resting on the carriage inside the magazine of the apparatus shown in fig. 12, p. 17, so that it could not have bent even under its own weight on heating). The specimen was then cooled from about 1150° C under 22,000 psi maximum fiber stress and at a rate of 3° to 5° C per minute. The specimen deformed as shown in figure 44. This, and other experiments, showed the deformation on cooling to be gradual and permanent with an approximately one to one correspondence with the thermal-expansion curve. No tendency for the specimen to straighten itself out was observed on cooling. The bent specimens are shown in figure 45. Specimen A was heated under load but cooled without load, whereas specimen B was heated without load but cooled under load. The calculated maximum fiber stress was the the same in both cases. Specimens made from hot-pressed pure zirconia (Z-O-HP, table II) behaved in a similar manner, as shown by the deflection-temperature curves in figure 46 and the photograph of the bent specimens in figure 47. It should be noted that after hot-pressing in a graphite die at 2025° C in vacuum, the originally pure zirconia becomes a cermet of zirconia and zirconium metal with most of the zirconium in the grain boundaries (see fig. 23).

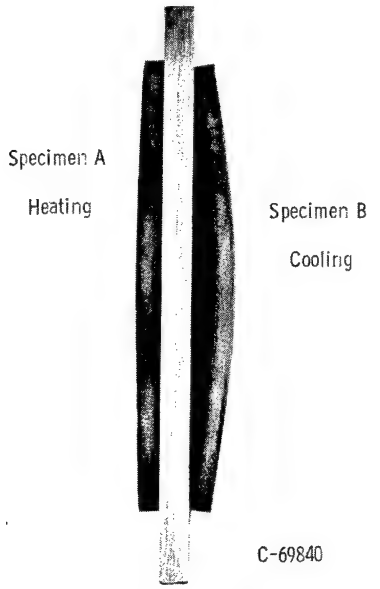

Figure 45. - Specimens of zirconia with 15 mole percent titanium (ZT-15-M) after cycling through transformation temperature. Center piece is a straight edge.

The deflections shown in figure 44 are actually plastic deformations, since the elastic component of the deformation is negligibly small by comparison. Although the curves include only the region about the transformation range, the plastic deformation outside this range was practically zero. The low-temperature ductility reported in reference 9 on this type of material could not be substantiated by

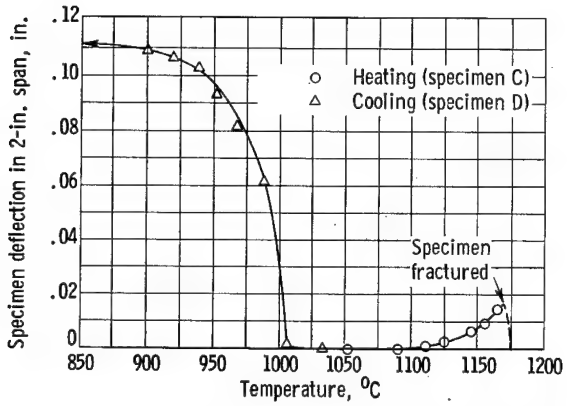

Figure 46. - Plastic deformation of vacuum hot-pressed zirconium oxide (Z-0-HP) on heating and cooling through transformation range. Specimen dimensions, 0.493 inch wide by 0.101 inch thick; maximum fiber stress, 12,000 psi; heating rate, 3.5° C per minute; cooling rate, 3.2° C per minute.

the preceding and similar experiments. No attempt has been made to investigate the low-temperature creep also reported in reference 9.

As shown in figure 44, the specimen deflection under load occurs at approximately the transformation temperature. The transformation temperature for the Z-0-HP specimen was (with the dilatometer) about 80° C higher than that of ZT-15-M. The relation between plastic deformation and transformation temperature in Z-0-HP was practically the same as that for ZT-15-M.

Although it has been stated that there is a correspondence between the thermal-expansion and the deflection curves, there may actually be a temperature difference between equivalent points in the two curves, but the type of thermocouples (W against W + 26 percent Re) and the equipment used were not sufficiently accurate to determine this difference.

One may inquire as to the actual amounts of plastic deformation involved in these experiments, since the degree to which the specimen can be bent depends on the thickness of the specimen.

The curvature of the specimens shown in figure 45 can be approximated by that of circular arcs of radius r,

$$r \simeq \frac{L^2}{8\delta} \tag{17}$$

where L is the span between rods, 2.000 inches, and δ is the deflection at the midspan of the bar. Letting d be the thickness of the bar (d = 0.100 in. in fig. 45) gives the elongation of the bottom fibers ΔL with respect to the neutral axis:

$$\Delta L = \frac{4d\delta}{L} \tag{18}$$

whence

$$\frac{\Delta L}{L} = \frac{4d\delta}{L^2} \tag{19}$$

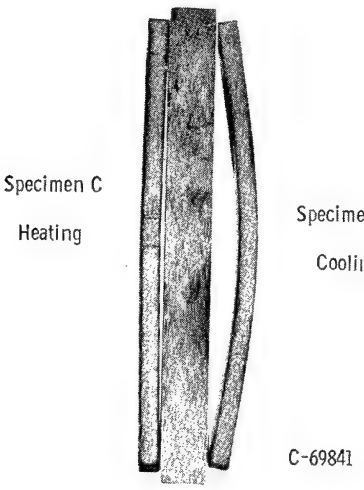

Figure 47. - Specimens of zirconia (Z-0-HP) after cycling through transformation temperature. Center piece is a straight edge.

With δ = 0.082 inch (from fig. 44),

$$\frac{\Delta L}{L} = \frac{4 \times 0.100 \times 0.082}{4} = 0.0082 \text{ in./in.} \tag{20}$$

or 0.82 percent plastic deformation for ZT-15-M at rupture during cooling.

As already stated, the behavior of the hot-pressed pure zirconia (Z-O-HP) was similar. Only one set of curves was obtained for this type of material (fig. 46). The specimen used for the heating cycle fractured so that it is not certain whether this material would have straightened itself out on continued heating (specimen C in figs. 46 and 47). On cooling another Z-O-HP specimen under load, it deformed just like that of ZT-15-M composition, but it underwent up to 1.11 percent outer fiber deformation without breaking (specimen D in figs. 46 and 47).

The elastoplastic behavior described in the previous paragraphs accounts for the observed discrepancy between the experimental and calculated ΔT. As can be ascertained from the thermal shock equations (eqs. (10) and (12), an increase in $\sigma_{\theta_{max}}$ or a decrease in E will increase ΔT. According to Griffith's theory, the low tensile strength of ceramics compared with their compressive strength is due to the stress-raising effect of cracks, and plasticity can be expected to increase $\sigma_{\theta_{max}}$ by relieving stress concentrations. On the other hand, the effects of plasticity could be introduced into the thermal shock equations by using a stress-dependent modulus of elasticity. This elastoplastic modulus would be lower than the purely elastic modulus in the presence of plasticity. Thus, the net effect of plasticity would be to raise ΔT. This elastoplastic behavior also accounts for the difference in the shape of the cracks developed on thermally shocking the specimens from below and through the transformation range, and for the bending of modulus-of-elasticity specimens.

The plastic deformation described appears to be a function of temperature, load, specimen size, and so forth, and a complete study of these variables is beyond the scope of this investigation.

To the writer's knowledge, this is the first time that such a plastic behavior through the transformation range of a ceramic has been observed, but this phenomenon is not new in the case of metals. Plastic deformation during the martensitic transformation of gold-cadmium single crystals has been described (ref. 31). Similar phenomena have been reported for the martensitic transformation in the indium-thallium system (refs. 32 and 33), for the martensitic transformation in iron alloys (ref. 34), and so forth. The plasticity in some of these alloys has been shown to be caused by twinning of one of the phases followed by the movement of the twinning plane under the influence of a shear stress. In some of these alloy systems, the twinned phase is the tetragonal phase. On the other hand, natural monoclinic zirconia is known to twin (ref. 35), and the possibility exists that the plasticity is due to the movement of a monoclinic twin interface.

An investigation of the twinning of the tetragonal phase would require the use of high-temperature microscopy or high-temperature X-ray equipment (Laue patterns), but because of the time involved in work of this nature it was not attempted. Some preliminary work was carried out to establish whether the monoclinic phase twins. Electron photomicrographs of bent specimens of ZT-15-M are shown in figures 48 and 49. Although some grains show an acicular and

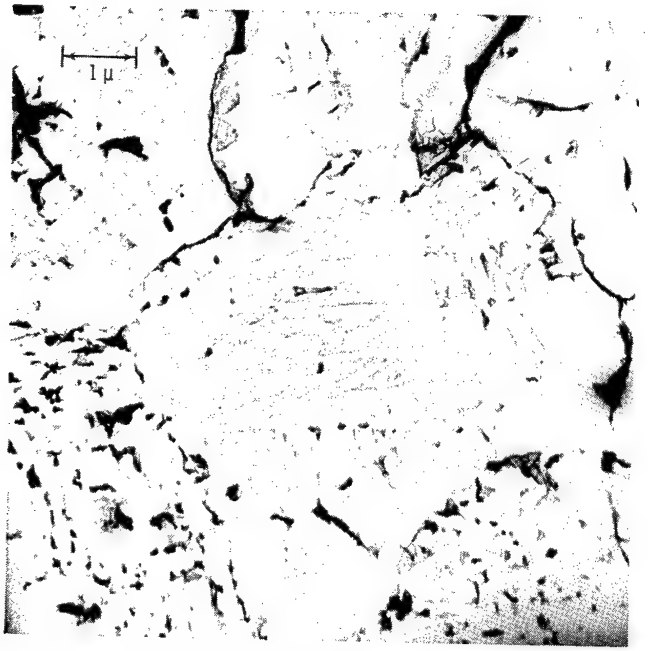

Figure 48. - Electron photomicrograph of deeply etched zirconia plus 15 mole percent titanium (ZT-15-M).

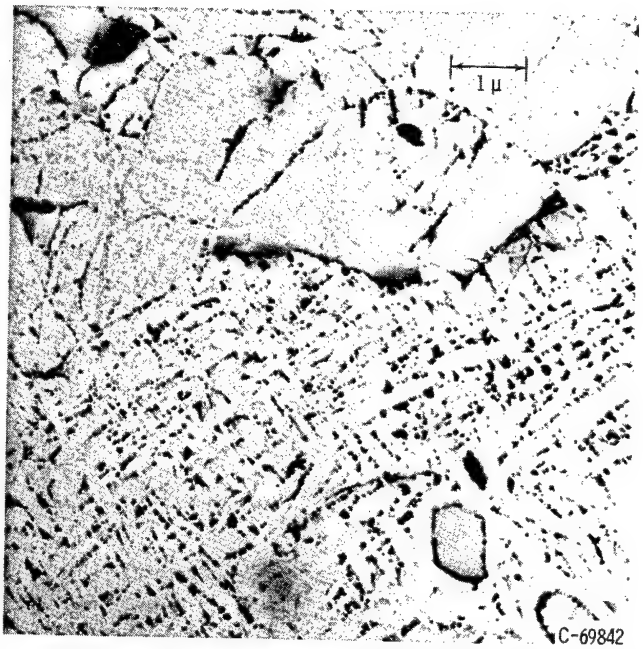

Figure 49. - Electron photomicrograph of deeply etched zirconia plus 15 mole percent titanium (ZT-15-M). Etched 5 minutes in concentrated hydrofluoric acid.

others a Widmanstatten type of structure, it is surmised that they may be etching artifacts. Attempts to obtain room-temperature Laue patterns of the same material failed because of the smallness of the grains. Consequently, the results of this part of the investigation are inclusive.

Considering that the transformation temperature is stress dependent (ref. 36), the plastic deformation could be explained, in part, by this effect, at least qualitatively. Thus, on heating, the applied stress would reduce the transformation temperature of the top fibers in the test bar causing them to shrink faster than the bottom fibers at first. Eventually, the bottom fibers would also transform causing the bar to straighten itself out. This mechanism, however, does not explain why the bar does not straighten itself out after transformation is completed when the specimen is bent on cooling.

Although the similarity of behavior between the zirconia-titanium (ZT-15-M) or zirconia-zirconium (Z-0-HP) compositions and martensitic alloys during transformation suggests that the zirconia in this composition transforms martensitically rather than by nucleation and growth, further work will be required before this point is clarified.

Whatever the transformation mechanism may be, however, atoms are displaced during the transformation with a concomitant volume change in the material. If a grain transforms, it and the adjacent grains will be under stress, and the grain will transform in such a way as to minimize this stress. The movement of these grains must involve a rather large amount of grain boundary sliding. For this reason, experiments were carried out in order to establish the nature of the grain boundaries in the zirconia-titanium compositions.

Nature of Grain Boundary in Zirconia with 15 Mole Percent Titanium

Milling and sintering experiments. - When zirconia-titanium compositions are milled, they become darker than the same compositions mixed thoroughly but not milled. Pellets of these compositions together with one of pure zirconia are shown in figure 50. The pure zirconia pellet is actually white, the mixed composition is light gray, and the milled composition dark gray. This shows that color depends on the degree of dispersion of the metal.

Pellets of these three compositions were individually vacuum sintered at successively higher temperatures up to the melting point. The specimens were polished and examined under the microscope.

Whereas the melting point of pure zirconia has been reported to be about 2700° C the (zirconium-rich) vacuum-sintered material melted at temperatures below 2620° C. Zirconia with 15 mole percent titanium, on the other hand, was observed to melt at about 2400° C. Actually, these melting points have very little meaning because they are probably not true equilibrium compositions. This lowering of the melting point was to be expected in view of the published zirconia-oxygen phase diagrams (refs. 20, 21, and 37). It appears from these experiments that titanium additions lower the melting point of zirconia just as excess zirconium does, although not necessarily in the same amount.

Pure vacuum-sintered zirconia was observed to change from white to a slightly yellowish light gray after sintering runs up to about 2150° C, at which temperature the sintered pellets were black. The change from white to light gray during sintering runs below about 2150° C is attributed to zirconium metal precipitating out on cooling through the 1580° C range, according to the zirconium-oxygen diagram of reference 37. This phase diagram is shown in figure 51 for ease of reference. Microstructures for the vacuum-sintered pure zirconia are shown in figure 43 (p. 35). The grain boundaries of the pellet sintered at 2400° C contain oxygen saturated zirconium metal (according to the phase diagram). No metal is visible in the specimens sintered at 1980° C and below. It is quite probable that the boundary metal forms on cooling through the solidus line in the phase diagram. Thus, the black color of these composi-

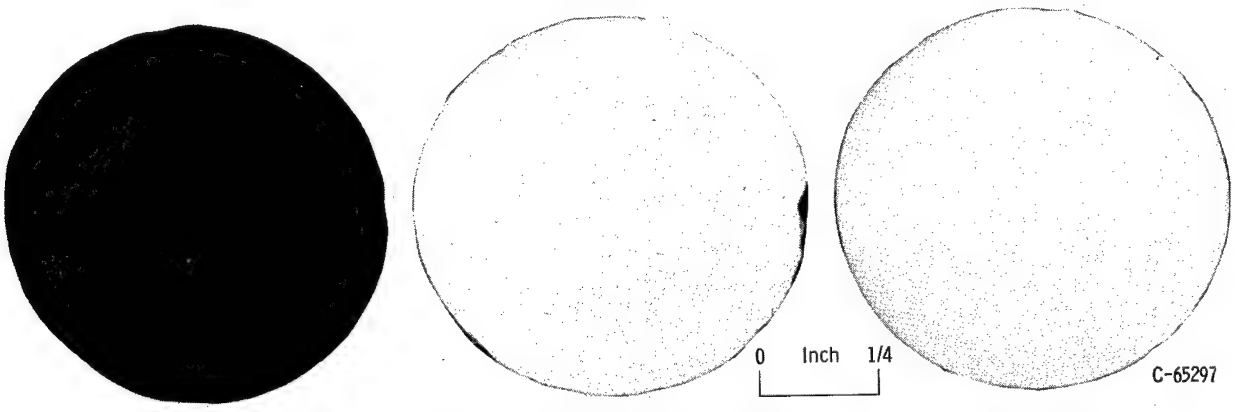

(a) Milled zirconia plus 15 mole percent titanium.

(b) Zirconia plus 15 mole percent titanium.

(c) Zirconia.

Figure 50. - Cold-pressed disks showing effect of composition and milling on color.

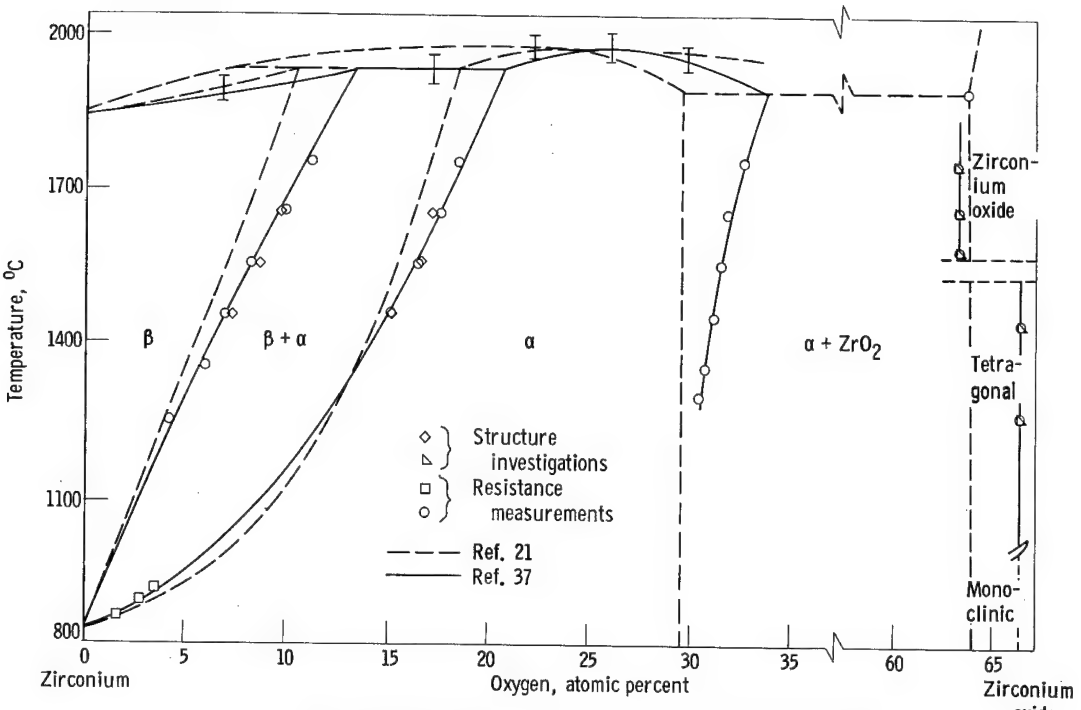

Figure 51. - Partial diagram of zirconium-oxygen system (ref. 37).

tions appears to be due to the metal in the grain boundaries. The microstructure of vacuum-melted originally pure zirconium oxide is shown in figure 43(d). This structure shows zirconium metal in the grain boundaries and a precipitate of lamellar zirconium, which resembles pearlite in structure.

The mixed zirconia with 15 mole percent titanium (ZT-15) darkened gradually as the sintering temperature was increased and became black in the range 1400° to 1600° C. The milled zirconia with 15 mole percent titanium became black on sintering below 1000° C for 1 hour. Up to near 2200° C, the microstructures are similar to those shown in figures 20 and 21 (p. 21), except for gradually increasing grain size.

Similar experiments showed nickel metal to blacken zirconia and titanium to blacken alumina and magnesia on vacuum sintering the ceramic - metal-powder compacts in the range 1000° to 1600° C for 1 hour. It seems quite probable from these experiments, that the black color of the zirconia-titanium compositions is not due to nonstoichiometry. The black color of these compositions probably is due either to the solubility of titanium in zirconia or to a coating of metallic titanium in the zirconia particles.

According to the work reported in reference 8, titanium dissolves substitutionally in zirconia, but the fact that the material becomes dark at such low temperature and dark gray on milling at room temperature precludes the possibility that the dark color is due to the titanium solubility in zirconium oxide, as this would require very large diffusion coefficients. Further, if titanium dissolves substitutionally in zirconia, the resulting structure would be equivalent to that obtained by mixing corresponding amounts of titania and zirconia. For low amounts of titania, these two oxides probably form a solid solution (ref. 2), and there is no reason to believe that its properties would

be much different from those of zirconia. Consequently, the assumption of reference 8 that the good thermal shock resistance of the zirconia-titanium compositions is due to the solubility of titanium in zirconia is questionable.

In order to test the second possibility, that is, that the black color of the material is due to coating of the particles, a series of tests were carried out.

Etching experiments. - Approximately 1-gram samples of the two types of zirconia with 15 mole percent titanium (ZT-15 and ZT-15-M) were sintered at various temperatures in vacuum, were crushed, and then finely ground in a mechanical tungsten-carbide mortar and pestle. These samples were digested for 24 hours in a strong acid (sulfuric, hydrochloric, or phosphoric appear to give about the same results). The acid slowly attacked the samples, which became lighter in color with increasing reaction time. The samples that had been sintered at low temperatures ($< 1500^{\circ}$ C) became a very light gray, whereas the samples that had been sintered at high temperatures became a darker gray (the higher the sintering temperature, the darker the powder). This showed that the black color of the samples was due to the presence of a distinct phase at the grain boundary, probably a titanium-zirconium-oxygen alloy. The gray color remaining after etching is attributed to trapped metallic particles or to patches of the dark grain boundary surrounded by normal zirconia-zirconia grain boundary.

Low-temperature sintering experiments. - Pellets of ZT-15 and ZT-15-M were vacuum sintered at 1000° C for 1 hour. The ZT-15-M sample was black; the ZT-15 sample was gray. The photomicrograph of ZT-15 is shown in figure 52.

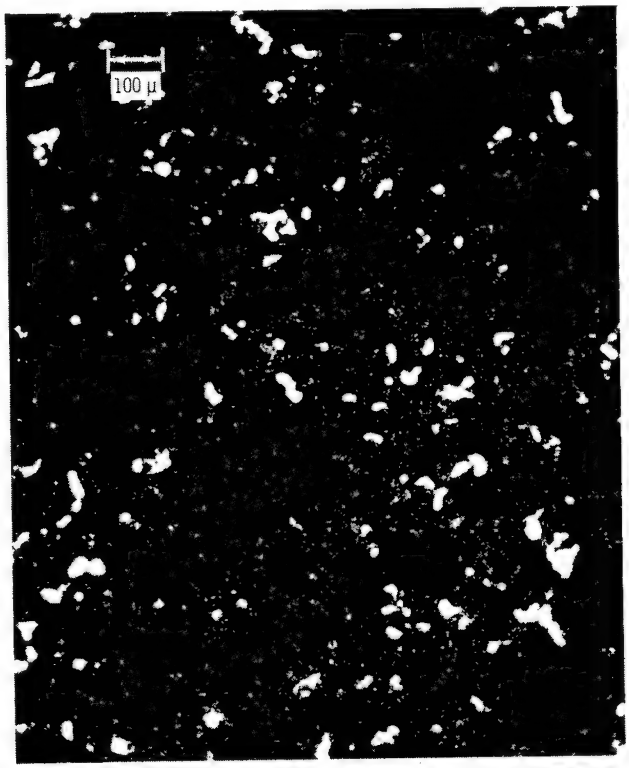

Figure 52. - Zirconia plus 15 mole percent titanium (ZT-15) vacuum sintered at 1000° C for 1 hour. Unetched.

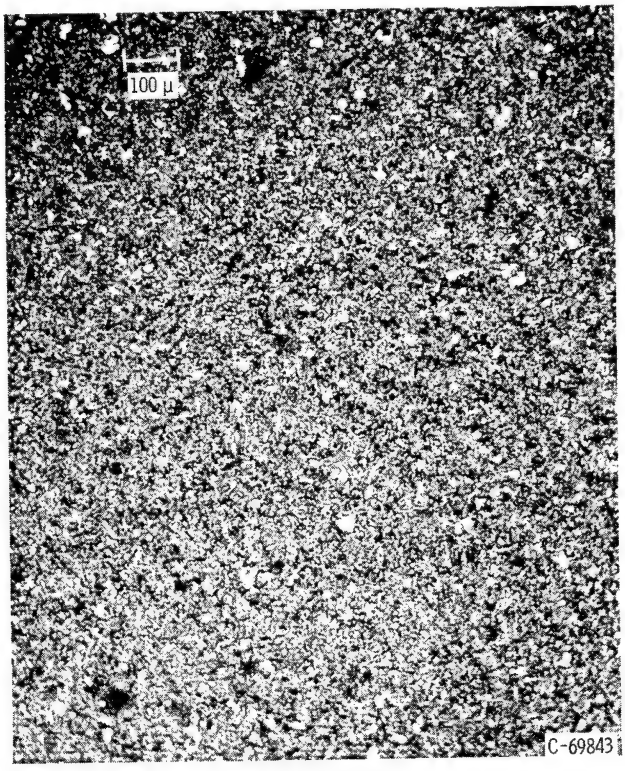

Figure 53. - Zirconia plus 15 mole percent titanium (ZT-15-M) vacuum hot-pressed at low temperature. Unetched.

The material immediately surrounding the metallic particles was dark and could be polished, whereas the material away from the metallic particles was lighter in color and was eroded away by the polishing operation. For this reason, the latter areas are out of focus in figure 52. The photomicrograph of ZT-15-M was uniformly dark in color and polished evenly. The structure was almost identical to that shown in figure 53 but more porous. The more uniform structure of the latter composition is attributed to the more rapid rate of coating of titanium on the zirconia particles due to the smaller particle size and greater degree of dispersion of the titanium in the milled composition.

After this series of experiments, it was reasonable to conclude that the black color of the material was due to the titanium (not necessarily pure) in the grain boundary. It has been shown in reference 8 that the metallic phase in the zirconia-titanium compositions is an alloy of titanium and zirconium oxide.

It should be noted that the zirconia grains need not be completely surrounded by the metallic phase in order to blacken the material or to inhibit grain growth. Although the experiments described herein indicate that the metallic grain boundary is fairly continuous it is surmised that the material retains a certain amount of normal zirconia-zirconia grain boundary, so that these compositions can retain a certain amount of strength even above the melting point of the metallic phase.

Low-temperature hot-pressing experiments. - In still another experiment, a composition of zirconia with 15 mole percent titanium milled by the same method used for ZT-15-M was loaded in a graphite hot-pressing die, cold-pressed into bars at 2000 psi in the same die, and vacuum sintered at 1000° to 1075° C (no pressure on the die) for 2 hours. After this time, the temperature was raised to 1280°±30° C and the material was hot-pressed at 2000 psi for 1 hour. The hot-pressed bars were ground to dimensions of 2.35 by 0.5 by 0.25 inch, and the modulus of rupture under three-point loading was determined.

The room-temperature modulus of rupture of these bars was 46,000 psi. The microstructure of this hot-pressed material is shown in figure 53. The density was 5.50 grams per cubic centimeter. Thus, despite the porosity of this material, its strength is higher than that of ZT-15-M, probably because of the fine grain size of the hot-pressed material.

It should be noted that the bars were hot-pressed above the transformation range and they did not crack on cooling. For this reason, the thermal shock resistance of this material is probably just as good as that of the other zirconia-titanium compositions. The significance of these findings is that this material was made below the temperature where a rapid change in zirconia stoichiometry occurs. According to reference 37, the oxygen content of zirconia changes from 63.5 to 66.5 atom percent on cooling through a temperature in the neighborhood of 1580° C in the phase diagram (see fig. 51, p. 42); consequently, the observed improvement in strength or thermal shock resistance cannot be attributed to α-zirconium precipitating out when the material is cooled through this temperature range.

From the hot-pressing experiment just described, it appears that in addition to initial particle size, final sintering temperature, and time at temper-

ature, properties of the material will also depend on the heating rate, since this will determine the amount of titanium coated or reacted in the would-be grain boundaries.

A metallic grain boundary, such as the one formed in the zirconia-titanium or zirconia-zirconium compositions, can allow grain boundary sliding because of the ductility of the metallic phase even if saturated with oxygen. On the other hand, the small grain size of the zirconia-titanium compositions (compare figs. 43(a), p. 35 and 21, p. 21) means a large specific grain boundary area and correspondingly smaller relative grain displacements. Large grains such as those shown in figures 23 or 24 (pp. 21 and 22) require correspondingly thicker metallic grain boundaries in order to prevent cracking on cooling through the transformation temperature. It should be pointed out that, for the small grain sizes of figures 20 or 21, the metallic grain boundary would be too thin to be visible in the light microscope even if all the metal were in the grain boundaries. The electron microscope cannot distinguish between grain boundaries with and without metal, but the deep etching of the grain boundaries in figure 48 (note the sheets of replica material pulled from the grain boundaries) suggests the presence of a different phase there. In addition to depositing in the grain boundaries, the metal is expected to help arrest crack propagation.

Thermal Shock Resistance of Zirconia with Other Metal Additions

If the thermal shock resistance of zirconia is due to the presence of a metallic grain boundary, there should be other metals besides titanium capable of improving the thermal shock resistance of zirconia (or other ceramics, for that matter).

What the properties of the metal should be are not known for certain, but it can be surmised that the metal should be fairly reactive so that the atoms will tend to adhere to the ceramic surface and form a layer of metal on it. In addition, the vapor pressure or surface diffusivity should be fairly high so as to form a coating on the ceramic particles in a reasonable time. Grain boundary diffusion may also play an important role in the particle-coating process.

In order to determine whether or not other metals have the same effect as titanium in improving the thermal shock resistance of zirconia, compositions of zirconia with 15 mole percent of metal were made by milling, cold-pressing, and sintering for 1 hour at 1870° C in vacuum at pressures lower than 0.5 micron of mercury. The metals used were zirconium, chromium, vanadium, silicon, tungsten, and molybdenum. In addition, a sample of hafnia with 15 mole percent titanium was made in the same manner. The designations for these compositions are shown in table II.

Zirconia bodies containing tungsten, molybdenum, and silicon could not be made. The samples made with tungsten or molybdenum invariably cracked despite very slow cooling rates. These samples were metallic dark gray probably reflecting the color of the metal powder, since zirconia is known to be translucent (ref. 38). The samples (disks) containing silicon were always cracked

even under very slow cooling. The disk had a light gray center tapering off to the light yellowish-gray color of vacuum-sintered pure zirconia at the edges. Microscopic examination showed that the gray center contained metallic particles of silicon with none at the edge. This effect is attributed to the high vapor pressure of silicon metal and perhaps suboxide formation in vacuum.

Compositions containing the other metals sintered normally. Zirconium tends to collect at the grain boundaries in thick layers (fig. 24, p. 22) and the structure is similar to that of vacuum hot-pressed pure zirconia (Z-O-HP, fig. 23, p. 21). Vanadium tends to behave in a similar manner (fig. 26, p. 22).

The structures of the zirconia-chromium (fig. 25, p. 22) and hafnia-titanium (fig. 27, p. 22) compositions are similar to that of ZT-15-M. These differences or similarities in structures may be due to metal reactivity, wettability, ability to restrain grain growth, and so forth, but this subject would require extensive study and will not be discussed any further.

The fact that disks of these compositions can be made at all indicates that the materials have reasonably good thermal shock resistance, otherwise they would crack on cooling through the transformation range (as does pure zirconia).

Disks of the previously named compositions ground to $1\frac{3}{8}$ inch diameter by 5/16 inch thick were thermally shocked in boiling water by the method already described. The results of the tests are shown in table III. These results are only approximate, since they represent averages of two tests and thermal shock tests usually show large scatter in the ΔT values. The results do show, however, that the theory of reference 8 that the improved thermal shock resistance of the zirconia-titanium compositions is due to the substitutional solid solution of titanium in zirconia can hardly be correct, for, as shown in table III, ZZ-15-M (made from zirconia and zirconium metal) has nearly the same thermal shock resistance as ZT-15-M (made from zirconia and titanium metal).

In addition to the compositions mentioned here, black bodies of zirconia with 8.2 volume percent nickel and of zirconia with 8.2 volume percent of a mixture of 60 weight percent molybdenum and 40 weight percent manganese were made by the low temperature hot-pressing techniques previously described. Although no quantitative thermal shock tests were carried out with these two compositions, the very fact that they could be cooled through the transformation range without cracking indicates that they have relatively good thermal shock resistance. It should be noted that the metals used in these experiments (particularly nickel) are less reactive than titanium, zirconium, vanadium, and chromium.

It should be pointed out that although tungsten, pure molybdenum, and silicon did not improve the thermal shock resistance of zirconia, it does not necessarily mean that they are unsuitable for this purpose, but perhaps rather that the technique used for coating the zirconia particles was incorrect. Thus, the previously described technique of low-temperature coating followed by low-temperature hot-pressing could prove to be suitable for silicon, and long-

time presintering at intermediate temperatures with larger zirconia or smaller metal particle size could be suitable for the zirconia-tungsten or zirconia-molybednum combinations.

From the experiments described, it can be concluded that titanium is by no means unique in its ability to improve the thermal shock resistance of zirconia.

SUMMARY OF RESULTS

The experimental thermal shock resistance of zirconia with 15 mole percent titanium was determined by quenching disks with thermally insulated faces. The thermal shock resistance of calcia-stabilized zirconia was also determined concurrently for comparison purposes. The effect of processing variables on the thermal shock resistance of the zirconia-titanium compositions was also investigated.

For quenches from below the transformation temperature, the thermal shock resistance of zirconia with 15 mole percent titanium was definitely better than that of stabilized zirconia. For quenches from above the transformation temperature, that of stabilized zirconia was slightly better.

Processing variables such as cold-pressing, milling, and sintering seem to have only a slight effect on the thermal shock resistance of zirconia with 15 mole percent titanium. In order to determine the reason for the improved thermal shock resistance of zirconia with titanium additions, the parameters that enter in the thermal shock equations were investigated. The parameters investigated as functions of temperature were heat capacity, thermal conductivity, coefficient of thermal expansion, modulus of rupture, and modulus of elasticity. In addition, the heat-transfer coefficient as a function of gas pressure was investigated.

Equipment to carry out the investigation of these parameters, as well as an apparatus for determining thermal shock resistance, was designed by the author. Illustrations and descriptions of the apparatus are included herein.

The heat capacity as a function of temperature was determined by the drop method. This heat capacity of the zirconia-titanium material was substantially the same as that of pure zirconia reported in the literature.

The thermal conductivity as a function of temperature was determined by the radial method. This thermal conductivity was consistently higher than that reported in the literature for calcia-stabilized zirconia. At room temperature, the thermal conductivity of the zirconia-titanium material was about three times that of stabilized zirconia but at about 1000° C this thermal conductivity was only about 30 percent higher. The higher low-temperature thermal conductivity appears to be an intrinsic property of monoclinic zirconia.

The transformation temperature range determined by thermal expansion was substantially the same as that reported in the literature, but the total ex- →

pansion as a result of the transformation was about twice the value reported. This discrepancy is attributed to the different materials used in the determination of the thermal expansion. The coefficient of linear thermal expansion was substantially the same as that reported in the literature for zirconia with 15 mole percent titanium.

The modulus of rupture was about 43,000 psi at room temperature. The curve for modulus of rupture against temperature shows a maximum at about 900° C where the modulus of rupture reaches a maximum of 60,000 psi. The modulus of rupture of stabilized zirconia was also determined. Comparison shows that the zirconia-titanium compositions have very high high-temperature values of modulus of rupture when compared with stabilized zirconia and are therefore useable to much higher temperatures in load-bearing applications. The low-temperature intrinsic modulus of rupture of zirconia-titanium compositions appears to be about the same as that of stabilized zirconia when corrections due to porosity and grain size differences are taken into account. The high-temperature strength of the zirconia-titanium compositions may be due either to the intrinsic strength of tetragonal zirconia or to the strengthening effects introduced by the metal.

The modulus of elasticity as a function of temperature was determined by measuring the deflection on bending prismatic bars. The modulus of elasticity of zirconia-titanium was consistently higher than the reported value for stabilized zirconia; however, the modulus of elasticity for stabilized zirconia reported in the literature had been determined on rather porous samples, whereas the material used in this investigation was nearly 100 percent dense. For this reason, no quantitative comparison can be made.

The values of the thermal shock parameter ΔT calculated from the preceding data were compared with the experimental values of ΔT. For quenches from below the transformation temperature, the calculated and experimental ΔT agreed reasonably well, whereas for quenches through the transformation temperature, the experimental ΔT was about seven times higher than the calculated values. This discrepancy was traced to plasticity in the transformation range. Careful modulus-of-elasticity determinations, together with the determination of the deformation at constant load and variable temperature, led to the discovery of a heretofore unreported elastoplastic behavior of zirconia. The zirconia-titanium material deformed plastically in the transformation range, both on heating and on cooling. This plastic behavior has been observed in metallic alloys that transform martensitically, but to the writer's knowledge, this is the first time that such behavior has been observed in a ceramic. The plastic behavior of the material accounts for the observed discrepancy between calculated and experimental values of ΔT through the transformation range.

The improved thermal shock resistance for zirconia-titanium compositions on quenching from below the transformation range was traced to the small grain size of these compositions as compared with that of stabilized or of metal-free zirconia. The reason for this is that the strength of the material increases as grain size decreases according to Knudsen's equation, whereas the modulus of elasticity, the coefficient of thermal expansion, and the thermal conductivity of the material are not significantly affected by grain size.

It was also discovered that the black color of the zirconia-titanium compositions is associated with the presence of titanium in the grain boundaries. It is surmised that this modified grain boundary provides the required ductility to allow grain boundary sliding. The titanium also inhibited grain growth and, consequently, also aids grain boundary sliding by increasing the specific grain boundary area. In addition, the titanium also improves thermal shock resistance by increasing the thermal conductivity of the composite and by acting as a crack arrester. It was also found that disks of zirconia with either zirconium, chromium, vanadium, nickel, or molybdenum-manganese alloy could be sintered without cracking. Although the thermal shock resistance of some of these compositions depended on the metal, the very fact that these compositions could be made without cracking (contrasted with pure zirconia) indicated that the thermal shock resistance of the zirconia was improved by the metal additions. End

CONCLUDING REMARKS

As a corollary on these results, it is concluded that the thermal shock resistance of many other ceramics could be improved by metal additions. Considering the chemical and structural similarity of the oxides of zirconium, hafnium, and thorium, it is surmised that the results of the present investigation are directly applicable, at most with minor changes, to hafnia and thoria.

From the results of the effects of titanium additions on the high-temperature strength of zirconia and from the fact that grain size reduction improves the mechanical properties of most materials, it is concluded that the techniques for coating ceramic particles with metals developed in this investigation should be useful for inhibiting grain growth and increasing the thermal shock resistance of other ceramics. The same techniques should be useful for inhibiting the grain growth of metals by coating metallic particles with suitable compounds. Needless to say, these techniques will be suitable only for specific metal-compound combinations, since the mutual solubility of the materials involved may actually enhance grain growth. The question of what combinations of materials are suitable for grain growth control or for improvement of thermal shock resistance is beyond the scope of the present investigation.

Lewis Research Center
National Aeronautics and Space Administration
Cleveland, Ohio, June 1, 1964

APPENDIX A

DETERMINATION OF SURFACE HEAT-TRANSFER COEFFICIENT

Theoretical Considerations

The temperature distribution in a disk with thermally insulated faces during transient heating or cooling is the same as the temperature distribution in an infinite cylinder of the same material and heated or cooled under the same conditions. An expression for the temperature distribution in the infinite cylinder is given in reference 39. In terms of dimensionless variables, this temperature distribution may be represented symbolically by

$$U = f(\beta, \xi, \tau) \tag{A1}$$

where U, β, ξ, and τ are dimensionless parameters defined by

$$U = \frac{T - T_f}{T_i - T_f} \tag{A2}$$

$$\beta = \frac{hr_m}{k} \tag{A3}$$

$$\xi = \frac{r}{r_m} \tag{A4}$$

$$\tau = \frac{at}{r_m^2} \tag{A5}$$

and

T temperature at any position r and time t

T_i initial temperature of specimen

h surface heat-transfer coefficient

r_m maximum radius of disk

k thermal conductivity

a thermal diffusivity

The thermal diffusivity a is defined by equation (5).

Solutions for U in terms of the preceding dimensionless parameters can be found in the literature in the forms of tables (ref. 14) and figures (ref. 40). In this work, only Russell's tables (ref. 14) will be used because they are given with sufficient significant figures to allow plotting of curves

with great accuracy. One of the plots used for the determination of h is shown in figure 6 (p. 12).

The theory just outlined applies only for quenches from below the transformation temperature of zirconia. On cooling through the transformation range of zirconia, heat is generated and, consequently, the method just discussed for the determination of h is not valid. It should be noted, however, that h is a surface property and as such should not differ appreciably from tetragonal to monoclinic zirconia. Now, since the transformation temperature of the compositions studied here starts at about 1000° C on heating and about 900° C on cooling, it is possible to determine h through the transformation range on cooling without actually transforming the specimen.

Apparatus and Procedure

The heat-transfer coefficient h as a function of gas pressure was determined in the same apparatus described in the body of the report for the determination of ΔT. The specimens used were disks of ZT-15-M (see table II) of the same dimensions as the specimens used for the determination of ΔT but with thermocouple holes 0.032 inch in diameter located at relative radii r/r_m of 0, 0.5, and 0.8. The bottom of these holes was located at the half-thickness of specimen.

Chromel-Alumel thermocouples swaged in 0.020-inch outside-diameter Inconel tubes were used for temperature measurements at the points indicated. These thermocouples were connected to temperature recorders.

The gas flow was adjusted to the desired pressure level and cooling curves like those shown in figure 5 (p. 12) were obtained. From these curves, h was calculated by two different methods.

The first method involved the cooling curves at two different points in the specimen. Cooling curves corresponding to relative radii of 0 and 0.8 were used almost exclusively. The procedure consisted in calculating the relative temperatures U_0 and $U_{0.8}$ at a given time t after the start of cooling. The intersection of these two values of U in the plot of figure 6 (p. 12) gave β and τ. The value of h was then calculated from equations (5), (A3), and (A5):

$$h = \frac{\tau \beta c_p \rho r_m}{t} \tag{A6}$$

The value of c_p in equation (A6) was determined in this investigation.

The other method used for the determination of h required the independent determination of the diffusivity a. The value of $U_{0.8}$ at any time t was determined from the cooling curve at $r/r_m = 0.8$. The value of τ was determined with equation (A5). The intersection of this τ, $U_{0.8}$ pair of values in the plot shown in figure 6 gave β from which h was determined by means of equation (A6).

In this investigation, only the values of h obtained by the last method described were used, but the discrepancy between the two methods is relatively small.

For quenches taking place inside the lower portion of the heating tube, the specimen of ZT-15-M used was quenched from a position in the furnace that was at 950° C when the hot zone was at the maximum temperature attainable (1180° C). The final temperature was taken as the temperature of the specimen after 1 hour in the quenching position in the lower part of the tube. During these tests, argon flow and furnace temperature were the same as during the actual ΔT determination.

APPENDIX B

DETERMINATION OF HEAT CAPACITY

The apparatus used in the determination of the heat capacity c_p is a version of the well-known drop calorimeter (fig. 7, p. 15). This apparatus features an Inconel sample carrier that keeps the specimen in an upright position and reduces heat losses while the specimen is falling into the receiver. The Inconel heating tube was heated in a vertical tube furnace provided with a temperature controller. The furnace was capable of reaching temperatures up to 1000° C. The receiver features a screen to cushion the impact of the falling specimen and, at the same time, triggers both the receiver cover and the flap door closed. This flap door is actuated by a spring and, since it closes very fast, the heat transfer from the furnace and sample carrier to the calorimeter is minimized. The water in the calorimeter is continuously stirred around the finned copper receiver by means of a magnetic stirrer. The temperature in the calorimeter is read by a differential thermometer adjusted to read in the range 25.00° to 30.00° C. Calorimeter temperature changes can be estimated to 0.001° C.

The sample used was made from milled and sintered zirconia with 15 mole percent titanium (ZT-15-M, table II) and measured 1/2 by 1/4 by $2\frac{1}{4}$ inches (max.). One end of the sample bar had a longitudinal hole about 1/16 inch in diameter for location of a 0.020-inch outside-diameter swaged Chromel-Alumel thermocouple. Since the samples used are prone to oxidation, all heating was carried out in argon.

The calorimeter was calibrated by means of cast ice cylinders made from distilled water and held in equilibrium with water in a Dewar flask for not less than 24 hours. The calorimeter was loaded with 500.00±0.01 grams of distilled water at a temperature that would allow optimum utilization of the 5° C range of the differential thermometer. The calorimeter was stoppered and the magnetic stirrer was started. Calorimeter temperature readings were taken at regular intervals for a period of 10 to 15 minutes. An ice cylinder of suitable size was removed from the Dewar flask (with tweezers held inside the same flask) and dropped into the calorimeter. Temperature readings were continued for another 30 minutes. The time-temperature curve for the calorimeter was plotted and the temperature rise determined as the difference in (extrapolated) temperatures before and after the drop. The weight of the ice cylinder was obtained by the difference in the weight of the calorimeter before and after the drop. A correction of 0.004 gram per square centimeter was applied to the weight of the ice cylinder for the film of water sticking to it. The water equivalent of the calorimeter was obtained from the equation

$$Q_C = \frac{W_i \, \Delta H_f + (T_f - 0)\overline{(c_p)}_w (W_i + W_f)}{T_i - T_f} \qquad \text{(B1)}$$

where

Q_C water equivalent of calorimeter, cal/°C

W_i corrected weight of ice, g

ΔH_f heat of fusion of water, 79.71 cal/g

T_f final temperature of calorimeter, °C

$\overline{(c_p)_w}$ average heat capacity of water between T_f and 0° C, cal/(g)(°C)

W_f weight of water film on ice, g (estimated)

T_i initial temperature of calorimeter, °C

The values of $\overline{(c_p)_w}$ and ΔH_f were obtained from the literature (ref. 19).

In order to determine the heat capacity of the ZT-15-M composition, the enthalpy as a function of temperature had to be determined. To do this, the sample was heated in the furnace to an equilibrium temperature that was measured with a thermocouple-potentiometer combination. Meanwhile, the temperature of the water-loaded calorimeter was being determined as a function of the time, as already explained. The specimen was dropped into the calorimeter, the calorimeter was quickly stoppered, and calorimeter temperature readings continued for another 30 minutes or so. Drops were made at regular specimen temperature intervals starting at about 53° C. From below 100° C, drops were made directly into the calorimeter without the receiver. The heat content of the sample was determined from the equation

$$\Delta H = \frac{Q_C \, \Delta T_C}{W_s} \tag{B2}$$

where

ΔH change in enthalpy of specimen per gram

Q_C water equivalent of calorimeter, cal/°C

ΔT_C temperature rise in calorimeter, °C

W_s weight of specimen, g

In order to keep ΔT_C within the 5° C range of the calorimeter, the sample had to be cut off gradually as the initial temperature of the sample was increased.

The ΔH values were plotted as a function of temperature and the c_p in the range 25° to 30° C determined. This c_p (0.104 cal/(g)(°C)) was used to obtain ΔH from 25° C. The corrected values of ΔH were replotted and the heat capacity c_p as a function of T was determined from the defining equation

$$c_p = \left(\frac{\partial \, \Delta H}{\partial T}\right)_p \tag{B3}$$

APPENDIX C

DETERMINATION OF THERMAL CONDUCTIVITY AND THERMAL DIFFUSIVITY

Thermal conductivity and thermal diffusivity were determined from room temperature to about 1100° C on cylinders of ZT-15-M (see table II) by the well-known radial method. Two versions of the same apparatus were used: one for the determination of the thermal conductivity in the room temperature to about 320° C range and the other for temperatures above this range. The low-temperature apparatus is shown in figure 8, and the high-temperature apparatus is shown in figure 9 (p. 16). Both apparatus have the common power supply shown in figure 10 (p. 16). Both apparatus used specimens of the same dimensions.

The specimens used in this investigation were cylinders 1.375 inches in outside diameter by 1.000 inch high with a center hole 23/64 inch in diameter for location of the heater and with 0.040-inch-diameter thermocouple holes located 0.294 and 0.662 inch from the axis of the cylinder. The top guard was made of the same material and dimensions, except that the thermocouple holes ran through the 1-inch thickness of the cylinder. These holes were made concentric with the corresponding thermocouple holes in the sample. The lower guard was also of the same material and dimensions but had no thermocouple holes. Guards and specimens were accurately ground to the same dimensions. The holes in the specimens and guards were made with an impact grinder. In order to make the assembly of the specimen and the two guards gas tight, they were stacked and alined temporarily with tungsten wires through the thermocouple holes and a steel mandrel through the center hole. The temporary assembly was placed in a tungsten sintering boat with a weight on top of the assembly and heated to 950° C for 6 hours in vacuum in order to weld the guards and specimen together. (This "welding" takes place because of evaporation of titanium from the material, but the weld is not very strong and the assembly must be handled with care.) The mandrel and tungsten wires were removed before placing the heater in the center hole of the assembly.

Low-Temperature Apparatus

The heater was made from 10-mil Nichrome wire wound on a 1/4-inch outside-diameter alumina tube on which a helical groove and radial holes 3 inches apart were made for locating and holding the Nichrome wire. The length of the wire used in the heater was about 4 feet. The heater was secured to the assembly with ceramic cement at the top and bottom. Nichrome wire voltage probes were welded to the heater.

The specimen-heater assembly was placed inside a 3-inch-long piece of brass tube and between two disks of silicone rubber. The brass tube was provided with inlet, outlet, and distributors for the cooling fluid. The whole system was sandwiched between two disks of ceramic fiber board and made rigid by a steel frame. Thermocouples and heater connections reached the outside through holes in the silicone rubber and ceramic fiber board.

The power supply consists of two voltage regulators in parallel with a total capacity of 120 volt-amperes, a 0- to 140-volt output variable voltage autotransformer, and a wattmeter of 240 watts capacity in six ranges. This wattmeter was calibrated at NASA laboratories and the indicated outputs are believed to be accurate to within ±1 percent.

The thermocouples used were Inconel sheathed 0.020-inch outside-diameter Chromel-Alumel. The thermocouples were checked for equality of emf output by placing them in a hole in a stainless-steel block, which was then heated in steps to 1100° C. The output of the individual thermocouples was measured with a precision potentiometer. On the basis of emf outputs, pairs of thermocouples were selected so that their readings differed by less than 0.1° C in the whole range. The thermocouples were also checked simultaneously against a platinum - platinum plus 10 percent rhodium thermocouple, and the reported temperature readings are believed to be accurate to within ±1° C.

Both water and helium were used as cooling fluids. For measurements in the range 20° to 120° C, water was used as the cooling fluid. The temperature level of measurement was varied by changing the power input or the water flow, or both. In the range from 120° to 320° C, helium was used as the cooling medium. The temperature level of measurements was changed by varying either the power input, the helium flow, or both. The temperature difference between thermocouples was kept at about 20° C. Measurements were taken under quasi-equilibrium conditions with the temperatures increasing or decreasing at less than 0.02° C per minute.

High-Temperature Apparatus

The same specimen-heater assembly was used except that a double-strand 5-mil thoriated tungsten wire was employed for the heater and voltage probes instead of the Nichrome wire. Tungsten wire had to be used because Nichrome heaters burned out very rapidly at high temperatures. Cooling takes place by radiation in vacuum or by radiation and convection in inert atmospheres. In this part of the investigation only vacuum was used.

The operating temperature level can be adjusted by either the input to the heater, by the input to the susceptor, or both. Although the temperature level can be adjusted in principle by the input to the heater alone, this method can be used only at relatively low temperatures (up to about 800° C), because, at high temperatures, the heat losses by radiation are high and the heaters burn out readily. On the other hand, high heat inputs imply high temperature drops across the specimen, which, if high enough, will cause cracking due to the high thermal stresses, particularly in the transformation range. For these reasons, the power input to the susceptor was adjusted so that the temperature difference between the two thermocouples was in the range from 20° to 50° C.

The thermocouples used were also Inconel sheathed 0.020-inch outside-diameter Chromel-Alumel and were calibrated in the same manner. The power supply used was also the same one used with the low-temperature apparatus.

In both cases, the thermal conductivity was determined from the equation (ref. 41).

$$k = \frac{\ln \frac{r_2}{r_1}}{2\pi} \frac{q}{T_1 - T_2} \qquad (C1)$$

where

k thermal conductivity, (cal)(cm)/(sec)(cm^2)(^oC)

r_2 distance of outer thermocouple from axis, cm

r_1 distance of inner thermocouple from axis, cm

q heat input per unit length of heater, cal/cm

T_1 temperature of inner thermocouple, ^oC

T_2 temperature of outer thermocouple, ^oC

The temperature of measurement was taken as the average between T_1 and T_2.

Even though k may vary with T, the difference between T_1 and T_2 is so (relatively) small that no appreciable error is introduced by the assumption that k is constant in the temperature range T_1 to T_2, as was done in equation (C1).

APPENDIX D

DETERMINATION OF THERMAL EXPANSION

The zirconia-titanium composition used in the present investigation was the type designated as ZT-15-M (table II). The dilatometer used is shown in figure 13 (p. 18). It can operate in vacuum or inert atmospheres at temperatures in excess of 2000° C.

The specimen holder is made of tungsten and is supported by three 1/4-inch-diameter ground tungsten rods welded to the base of the holder. These rods are fastened to the water-cooled brass cover by collars held in place with set screws. The openings for these rods in the cover are provided with O-ring gaskets. The expansion of the specimen is transmitted to a dial gage by a 1/4-inch ground tungsten rod free to move up and down (or rotate) in accurately machined holes in the tungsten specimen holder cover and water-cooled brass cover. The opening in the latter is provided with an O-ring gasket. The movement of the rod is transmitted to the dial gage through an adjustable arm. The dial gage has a range of 0.400 inch and is calibrated in 0.0001-inch divisions. The specimen holder can accommodate specimens up to 1 inch in diameter by $3\frac{1}{2}$ inches long.

Temperatures are measured by a thermocouple inside a 1/4-inch outside-diameter molybdenum tube that passes through a vacuum feed-through fitting in the brass cover and reaches inside the specimen holder. The thermocouple wires pass through another fitting brazed to the top of the molybdenum tube. The thermocouple assembly can be removed from the hot zone without breaking the vacuum. Temperatures can also be measured with an optical pyrometer by sighting through a glass prism in the brass cover.

The specimen is heated by a susceptor that is heated by induction. In order to obtain a uniform temperature distribution, the susceptor and the specimen holder assembly are provided with tungsten radiation shields and stabilized-zirconia insulation, as shown in figure 13 (p. 18).

The dilatometer can be fitted with a glass bell if desired so that the O-rings used for sealing the assembly vacuum tight can be dispensed with and frictional effects on the actuating rod minimized. Actually, this friction on a well-lubricated rod is negligible and the bell has not been used in this work. Because of its large range, the dilatometer can also be used to study sintering shrinkage as a function of time and temperature. The actuating rod protrudes through a hole in the bridge to which the dial is fastened. By placing weights on this rod, the dilatometer can also be used to study transformation kinetics (ref. 32). In order to use the dilatometer, the expansion of the apparatus proper as a function of temperature must be known. This can be accomplished by means of a standard of known thermal expansion. The standard used in this study was tungsten. The thermal expansion of this material was taken from the literature (ref. 42). The thermal expansion of the dilatometer for the given length of standard is

$$\Delta L_D = \Delta L_{St} - \Delta L_G \tag{D1}$$

where

ΔL_D expansion of dilatometer

ΔL_{St} expansion of standard

ΔL_G change in gage reading

The dilatometer was calibrated with a 3.000-inch-long by 1/4-inch-diameter tungsten rod by the same procedure to be described for specimens.

All thermal expansion work was carried out in a vacuum at better than 0.5 micron of mercury. The specimen used was 3.000 inches long by 0.400 inch wide by 0.400 inch thick, squared and ground all over. As already stated, the material used was that designated as ZT-15-M (zirconia with 15 mole percent titanium that had been milled, cold-pressed, and sintered).

Dial gage readings were taken near equilibrium temperatures with heating and cooling rates of less than 0.1° C per minute. Temperatures were determined both with a tungsten against tungsten plus 26 percent rhenium thermocouple and also with a disappearing-filament optical pyrometer. The thermocouple was guaranteed accurate to within 1 percent by the supplier.

The thermal expansion was determined from

$$\Delta L = \frac{1}{3} (\Delta L_D + \Delta L_G) \tag{D2}$$

where

ΔL expansion of sample from room temperature to given temperature, in./in.

ΔL_G expansion of system, as measured by deflectometer, from room temperature to given temperature, in.

ΔL_D expansion of deflectometer from room temperature to given temperature as given by equation (D1), in.

The factor 1/3 in equation (D2) was used because the length of the standard and specimen were both 3.000 inches.

APPENDIX E

DETERMINATION OF MODULUS OF RUPTURE IN BENDING

The room-temperature modulus of rupture was carried out in standard types of fixtures (ref. 25) both for three- and four-point loading. The modulus of rupture above room temperature was carried out in vacuum in a semiautomatic modulus-of-rupture fixture (fig. 12, p. 17). The details of its construction and operation have already been described (ref. 13).

For the determination of the modulus of rupture at room temperature under four-point loading, prismatic bar specimens 6 inches long by 1/2 inch wide in several thicknesses from 0.100 to 0.300 inch were made from milled zirconia with 15 mole percent titanium by the procedures already described. These specimens had a surface finish of 50 microinches. Experimentally, the modulus of rupture does not appear to be significantly affected by small changes in the distance between the points of application of the load (ref. 10) and, consequently, is not expected to be significantly affected by small changes in width, since in Weibull's theory, both length and width contribute to the volume under stress in the same manner.

For room-temperature three-point-loading and for high-temperature three-point-loading modulus of rupture, bars 2.35 inches long by 0.500 inch wide by 0.250 inch high of the same material were used. These specimens were polished metallographically on the bottom and side surfaces in order to remove possible stress raisers. The same type of three-point-loading specimens were made from the mixed and sintered zirconia with 15 mole percent titanium (ZT-15) and from milled calcia-stabilized zirconia (BM, table II).

The specimens were loaded at maximum fiber stress rates between 50,000 and 150,000 psi per minute. The effect of stress rate does not appreciably affect the modulus-of-rupture values at these stress-rate levels (ref. 43).

During the determination of the modulus of rupture under three-point loading at other than room temperature, the specimens were held 20 minutes at the test temperature before applying the load.

On four-point-loading room-temperature testing, the modulus of rupture with distances of 1, 2, and 4 inches between the points of application of the load were determined, with two specimens for each thickness tested. In all cases, the modulus of rupture was determined from the well-known equation

$$\sigma_M = \frac{3}{2}\frac{PL}{bd^2} \qquad (E1)$$

where

σ_M modulus of rupture

P load, lb

L length of beam under three-point loading and twice distance from a support point to nearest point of application of load under four-point loading

b width of specimen, in.

d height of specimen, in.

APPENDIX F

DETERMINATION OF YOUNG'S MODULUS OF ELASTICITY

The apparatus used to determine the Young's modulus of elasticity in bending is shown in figure 13 (p. 18). This apparatus is similar in construction to the modulus-of-rupture apparatus (fig. 12, p. 17); in fact, the same housing and a few other parts are common to both. This apparatus is also made entirely of graphite. The furnace used in conjunction with this tester is shown in figure 3 (p. 7). No modifications are required in the furnace in order to change from modulus-of-rupture to modulus-of-elasticity testing.

In the modulus-of-elasticity apparatus shown in figure 13, the test specimens are bent on a 4.000-inch span by pushing at the midspan of the specimen with a push rod attached to the crosshead of the tensile machine through collars, rods, and couplings as for the modulus-of-rupture apparatus. The push rod is prevented from rotating by means of a set screw.

Either two specimens or a specimen and a standard are located on two 1/2-inch-diameter graphite rods that are attached to a carriage by graphite pins.

This carriage can move back and forth in a track cut in the base when actuated by the arm attached to the actuator extension rod which, just as in the case of the modulus-of-rupture apparatus, can be rotated from outside the furnace so that either one or the other of the test bars are in the bending position under the push rod. The rods on which the test bars ride move back and forth with the carriage in V-grooves in the base. The test bars are separated from each other and from the carriage by means of locating pins. The bottoms of the test bars clear the carriage by 0.010 to 0.040 inch (depending on dimensions of specimen) so as to prevent the specimens from breaking if the load corresponding to a predetermined stress level is exceeded. The load and the crosshead position are recorded in the tensile machine recorder.

The temperature can be determined either optically or with a tungsten against tungsten plus 26 percent rhenium thermocouple.

The modulus of elasticity in compression was determined on cylinders of ZT-15-M provided with strain gages. Two strain gages in series, 180° apart were used to measure vertical deflections. Two strain gages in series, also 180° apart, were used to measure horizontal deflections. Loads were applied by a compression testing machine. Strains were measured with a commercial strain indicator.

The setup used to determine the dynamic modulus of elasticity is the same as that described in reference 29 except that no furnace was used in this investigation.

The modulus of elasticity in bending was determined in prismatic bars of zirconia with 15 mole percent titanium, milled, cold-pressed and sintered

(ZT-15-M), and ground to final nominal dimensions of $4\frac{7}{8}$ inches long by 3/4 inch wide by 1/8 to 1/4 inch thick. The standard used was a prismatic bar of tungsten $4\frac{7}{8}$ inches long by 3/4 inch wide by 1/2 inch thick.

The specimens were held at temperature for 20 minutes and loads applied at a rate of about 10,000 psi per minute. Several load-deflection curves were determined at each temperature for both the specimen and the standard.

The use of a standard is required because the deflectometer registers total crosshead movements and includes the elongation of the tensile machine screws, the shortening of the furnace plungers, rods, carbon plug, and so forth, in addition to the deflection of the specimen. These elongations and compressions will be the same for the specimen and for the standard.

From the pure deflection of the specimen δ_s, Young's modulus of elasticity is given by the following equation from reference 17,

$$\delta_s = \frac{PL^3}{48E_sI_s} \tag{F1}$$

where

δ_s midspan deflection, in.

P load, lb

L span, in. = 4.000 in.

E_s Young's modulus, psi

I_s moment of inertia of cross section of beam

The actually measured deflection under the load P will be

$$\delta_{ms} = \delta_s + \delta_f \tag{F2}$$

where

δ_{ms} measured deflection with specimen, in.

δ_s specimen deflection, in.

δ_f furnace and fixture displacement, in.

Similarly, the deflection of the standard δ_n will be

$$\delta_n = \frac{PL^3}{48E_nI_n} \tag{F3}$$

where the subscript n means standard. In this case, the total deflection under the same load P will be

$$\delta_{mn} = \delta_n + \delta_f \tag{F4}$$

where

δ_{mn} measured deflection with standard, in.

δ_n calculated standard deflection (eq. (F3)), in.

δ_f furnace and fixture displacement, in.

Then, from equations (F3) and (F4),

$$\delta_f = \delta_{mn} - \delta_n = \delta_{mn} - \frac{PL^3}{48E_nI_n} \tag{F5}$$

and from equations (F1), (F3), and (F5)

$$\delta_s = \delta_{ms} - \delta_{mn} + \frac{PL^3}{48E_nI_n} = \frac{PL^3}{48E_sI_s} \tag{F6}$$

whence

$$E_s = \frac{PL^3}{48I_s\left(\delta_{ms} - \delta_{mn} + \frac{PL^3}{48E_nI_n}\right)} \tag{F7}$$

Actually, a value ΔP as shown in figure 36 (p. 27) rather than an absolute value of P was used so as to utilize the straight portion of the deflection curve.

The modulus-of-elasticity standard used in this investigation was tungsten, and its modulus of elasticity as a function of temperature was taken from the literature (ref. 44). Actually, the use of a standard of known modulus of elasticity is not indispensable. The correction to be applied for the displacement of the furnace and fixtures δ_f can also be obtained by using two specimens of the same material of unknown Young's modulus. The two specimens must have different moments of inertia that can be easily accomplished by varying the thickness of the specimen. Using a similar analysis yields

$$E_s = \frac{PL^3}{48\left(\delta_{m,1} - \delta_{m,2}\right)}\left(\frac{1}{I_1} - \frac{1}{I_2}\right) \tag{F8}$$

where

$\delta_{m,1}$ deflection under load P with specimen 1

$\delta_{m,2}$ deflection under load P with specimen 2

I_1 moment of inertia of specimen 1

I_2 moment of inertia of specimen 2

The modulus of elasticity in compression at room temperature was determined on $1\frac{3}{8}$-inch-diameter by $1\frac{1}{4}$-inch-long specimens of ZT-15-M between two mild steel specimens of the same dimensions. The specimens were loaded and unloaded several times before readings were taken. The modulus of elasticity was determined by the equation

$$E = \frac{\sigma}{\epsilon_y} \tag{F9}$$

where

E Young's modulus, psi

σ applied compressive stress, psi

ϵ_y axial displacement, in.

As already stated in the body of the report, during the compression tests, the vertical (axial) and horizontal (diametrical) displacements were determined by strain gages (see fig. 38, p. 27). From these displacements, the axial strain ϵ_y and the diametrical strain ϵ_x were obtained. From these, Poisson's ratio ν was evaluated (ref. 17).

The modulus of elasticity at room temperature by the sonic method was determined on prismatical bar specimens 4.7162 by 0.4612 by 0.1032 inch with a density of 5.65 grams per cubic centimeter. The resonance frequency was 1130 cycles per second. The modulus of elasticity was determined from the equations given in reference 45.

REFERENCES

1. Johnson, J. R.: Development of a Cubic Oxide Protective Film on Zirconium. ORNL-2029, Oak Ridge Nat. Lab., Feb. 21, 1956.

2. Weber, B. C., Garrett, H. J., Mauer, F. A., and Schwartz, M. A.: Observations on the Stabilization of Zirconia. Jour. Am. Ceramic Soc., vol. 39, no. 6, June 1, 1956, pp. 197-207.

3. Stocker, J.: Comment on the Stabilization of Cubic Zirconia. Société Chimique de France Bull. vol. 28, Jan. 1961, pp. 78-79. (See also Henry Brutcher trans. 5259.)

4. Ryshkewitch, Eugen: Oxide Ceramics. Academic Press, 1960.

5. Buckley, John D.: Deterioration of Calcia-Stabilized Zirconia. NASA TN D-1595, 1962.

6. Weber, Berthold C., and Schwartz, Murray A.: Zirconia: Its Crystallographic Polymorphy and High-Temperature Potentials. TR 58-646, WADC, July 1958.

7. Weber, Berthold C., Thompson, William M., Bielstein, Hans O., and Schwartz, Murray A.: Ceramic Crucible for Melting Titanium. WADC TR 56-372, WADC, Sept. 1956.

8. Ruh, Robert: Reactions of Zirconia and Titanium at Elevated Temperatures. Ph.D. Thesis, Rutgers-The State Univ., 1960.

9. Pulliam, George R., and Leonard, Bruce G.: Influence of Environment on Ceramic Properties. TR-60-338, WADD, Oct. 1960.

10. Manson, S. S., and Smith, R. W.: Quantitative Evaluation of Thermal-Shock Resistance. Trans. ASME, vol. 78, no. 3, Apr. 1956, pp. 533-544.

11. Kingery, W. D.: Factors affecting the Thermal Stress Resistance of Ceramic Materials. Jour. Am. Ceramic Soc., vol. 38, no. 1, Jan. 1, 1955, pp. 3-15.

12. Buessem, W. R.: Thermal Shock. High-Temperature Technology, I. E. Campbell, ed., John Wiley & Sons, 1956.

13. Arias, A.: Semiautomatic Modulus of Rupture Tester for Operation in Vacuum or Inert Atmospheres. Rev. Sci. Instr., vol. 34, no. 8, Aug. 1963, pp. 911-914.

14. Russell, T. F.: First Report Alloy Steel Research Committee. Iron and Steel Reprint, May 1941. Tables reproduced in Austin, J. B.: The Flow of Heat in Metals. ASM, Cleveland, 1942.

15. Jaeger, J. C.: On Thermal Stresses in Circular Cylinders. Phil. Magazine, ser. 7, vol. 36, no. 257, June 1945, pp. 418-428.

16. Grain, Clark F., and Campbell, William J.: Thermal Expansion and Phase Inversion of Six Refractory Oxides. BM-RI-5982, 1962. Bur. Mines.

17. Timoshenko, S., and Goodier, J. N.: Theory of Elasticity. Second ed., McGraw-Hill Book Co., Inc., 1951.

18. Arthur, James S.: The Specific Heats of MgO, TiO_2, and ZrO_2 at High Temperatures. Jour. Appl. Phys., vol. 21, no. 8, Aug. 1950, pp. 732-733.

19. Kubaschewski, O., and Evans, E. L.: Metallurgical Thermochemistry. Pergamon Press, 1958.

20. Cubicciotti, Daniel: The Melting Point-Composition Diagram of the Zirconium-Oxygen System. Jour. Am. Chem. Soc., vol. 73, no. 5, May 1951, pp. 2032-2035.

21. Domagala, R. F., and McPherson, D. J.: System Zirconium-Oxygen. Trans. AIME, vol. 200, Feb. 1954, pp. 238-246.

22. Mauer, F. A., and Bolz, L. H.: Thermal Expansion of Cermet Components by High-Temperature X-Ray Diffraction. Rep. 4884 (PR12), NBS, June 15, 1956.

23. Rao, C. N. R., Turner A., and Honig, J. M.: Some Observations Concerning the Effect of Impurities on the Anatase-Rutile Transition. Phys. and Chem. of Solids, vol. 11, 1959, pp. 173-174.

24. Yoganarasimhan, S. R., and Rao, C. N. R.: Mechanism of Crystal Structure Transformations. Trans. Faraday Soc., vol. 58, 1962, pp. 1579-1589.

25. Duckworth, W. H.: Precise Tensile Properties of Ceramic Bodies. Jour. Am. Ceramic Soc., vol. 34, no. 1, Jan. 1951, pp. 1-9.

26. Kingery, W. D.: Introduction to Ceramics. John Wiley & Sons, Inc., 1960.

27. Knudsen, F. P.: Dependence of Mechanical Strength of Brittle Polycrystalline Specimens on Porosity and Grain Size. Jour. Am. Ceramic Soc., vol. 42, no. 8, 1959, pp. 376-384.

28. Spriggs, R. M., and Vasilos, T.: Effect of Grain Size and Porosity on the Transverse Bend Strength and Elastic Modulus of Hot-Pressed Alumina and Magnesia. Paper Presented at Meeting of Am. Ceramic Soc., Toronto (Canada), Apr. 24, 1961.

29. Wachtman, J. B., and Lam, D. G., Jr.: Young's Modulus of Various Refractory Materials as a Function of Temperature. Jour. Am. Ceramic Soc., vol. 42, no. 5, 1959, pp. 254-260.

30. Lyman, Taylor, ed.: Metals Handbook. A.S.M., 1948.

31. Chang, L. C., and Read, T. A.: Plastic Deformation and Diffusionless Phase Changes in Metals - The Gold-Cadmium Beta Phase. Trans. AIME, vol. 191, Jan. 1951, pp. 47-52.

32. Burkart, M. W., and Read, T. A.: Diffusionless Phase Change in the Indium-Thallium System. Trans. AIME, vol. 197, nov. 1953, pp. 1516-1524.

33. Basinski, Z. S., and Christian, J. W.: Experiments on the Martensitic Transformation in Single Crystals of Indium-Thallium Alloys. Acta Met., vol. 2, no. 1, Jan. 1954, pp. 148-166.

34. Breedis, J. F., and Robertson, W. D.: Martinsitic Transformation and Plastic Deformation in Iron Alloy Single Crystals. Acta Met., vol. 11, no. 6, June 1963, pp. 547-559.

35. McCullough, J. D., and Trueblood, K. N.: The Crystal Structure of Baddeleyite (Monoclinic ZrO_2). Acta Cryst., vol. 12, 1959, pp. 507-511.

36. Whitney, E. Dow: Effect of Pressure on Monoclinic-Tetragonal Transition of Zirconia; Thermodynamics. Jour. Am. Ceramic Soc., vol. 45, no. 12, Dec. 1962, pp. 612-613.

37. Gebhardt, Erich, Seghezzi, Hans-Dieter., und Dürrschnabel, Wolfgang: Untersuchungen in System Zirkonium-Sauerstoff, II. Jour. Nuclear Materials, vol. 4, no. 3, 1961, pp. 255-268.

38. Bliton, J. L., Rechter, H. L., and Harada, Y.: Flame Sprayed Zirconia Films for Fuel Cell Components. Am. Ceramic Soc. Bull., vol. 42, no. 1, Jan. 1963, pp. 6-9.

39. Carslaw, H. S., and Jaeger, J. C.: Conduction of Heat in Solids. Second ed., Oxford Univ. Press, 1959.

40. Heisler, M. P.: Temperature Charts for Induction and Constant Temperature Heating. Trans. ASME, vol. 69, Apr. 1947, pp. 227-236.

41. Worthing, A. G., and Halliday, D.: Heat. John Wiley & Sons, Inc., 1948.

42. Goldsmith, Alexander, Waterman, Thomas E., and Hirschhorn, Harry J.: Thermophysical Properties of Solid Materials. Vol. 1 - Elements. TR 58-476, WADC, Aug. 1960.

43. Shevlin, T. S., and Lindenthal, J. W.: Modulus of Rupture Versus Rate of Loading. Am. Ceramic Soc. Bull., vol. 38, no. 10, Oct. 1959, pp. 491-492.

44. Grossman, L. N.: Thermophysical Properties of Some Materials. Rep. GEAP 3734, General Electric Co., 1961.

45. Wachtman, John B., and Maxwell, Laurel H.: Factors Controlling Resistance to Deformation and Mechanical Failure in Polycrystalline (Glass-Free) Ceramics. TR-57-526, WADC, Dec. 1957.

TABLE I. - CHEMICAL COMPOSITION, PARTICLE SIZE, AND SUPPLY SOURCE OF RAW MATERIALS

Material	Supplier's designation	Supplier (a)	Composition, percent	Original particle size	Method of analysis
Zirconium oxide	CP Zirox	A	98.8 ZrO_2 (includes HfO_2), 0.33 Si, 0.10 TiO_2, 0.10 CaO	0.26 μ	B.E.T.
Zirconium oxide (stabilized)	Zircoa B	B	92.5 ZrO_2 (includes HfO_2), 5.33 CaO, 0.63 MgO, 0.50 Al_2O_3, 0.37 SiO_2	10 μ	------
Hafnium oxide	Grade II	C	95 HfO_2 approx.	-325 Mesh	Sieve
Titanium powder	--------	D	98 Ti, 1.1 N	-325 Mesh	Sieve
Zirconium powder	--------	D	98 Zr (includes 2 to 3 Hf)	-200 Mesh	Sieve
Chromium powder	Electrolytic	E	99.0 Cr, min.	-300 Mesh	Sieve
Vanadium powder	----------	F	99.7 V	20 Mesh	Sieve
Silicon powder	----------	E	97 Si, min.	-100 Mesh	Sieve
Molybdenum powder	----------	G	>99 Mo	4.5 μ	Fisher
Tungsten powder	----------	G	>99.5 W	1.15 μ	Fisher

[a]Qualified requesters may obtain a key to this column.

TABLE II. - DESIGNATION, COMPOSITION, AND TREATMENT OF SAMPLES

Designation	Composition	Treatment	Density, g/cc	Photomicrograph (pp. 21 and 22)
ZT-15	Zirconia + 15 mole percent titanium	Mixed, cold-pressed, vacuum sintered at 1870° C for 1 hr	5.20 to 5.27	Fig. 21
ZT-15-M	Zirconia + 15 mole percent titanium	Milled, cold-pressed, vacuum sintered at 1870° C for 1 hr	5.65 to 5.75	Fig. 20
ZT-15-HP	Zirconia + 15 mole percent titanium	Mixed, and vacuum hot-pressed at 1600° C and 2000 psi for 1 hr	5.30 to 5.60	Fig. 22
Z-O-HP	Zirconia	Vacuum hot-pressed at 2025° C and 2000 psi for 1 hr	5.81	Fig. 23
ZZ-15-M	Zirconia + 15 mole percent zirconium	Milled, cold-pressed, and vacuum sintered at 1870° C for 1 hr	5.82	Fig. 24
ZCr-15-M	Zirconia + 15 mole percent chromium	↓	5.82	Fig. 25
ZV-15-M	Zirconia + 15 mole percent vanadium	↓	5.80	Fig. 26
ZM-15-M	Zirconia + 15 mole percent molybdenum	↓	----	-------
ZS-15-M	Zirconia + 15 mole percent silicon	↓	----	-------
ZW-15-M	Zirconia + 15 mole percent tungsten	↓	----	-------
HT-15-M	Hafnia + 15 mole percent titanium	↓	9.22	Fig. 27
BM	Calcia-stabilized zirconia (Zircoa B)	Milled, cold-pressed, and air sintered at 1800° C for 3 hr	5.22	Fig. 28

TABLE III. - THERMAL SHOCK RESISTANCE OF VARIOUS COMPOSITIONS QUENCHES IN BOILING WATER

Designation	Composition	Thermal shock parameter, ΔT, °C
HT-15-M	Hafnia + 15 mole percent titanium	138
ZCr-15-M	Zirconia + 15 mole percent chromium	220
ZT-15-M	Zirconia + 15 mole percent titanium	350
ZV-15-M	Zirconia + 15 mole percent vanadium	81
ZZ-15-M	Zirconia + 15 mole percent zirconium	299
Z-O-HP	Zirconia	159

NASA-Langley, 1964 E-2348

NASA TN D-2464
National Aeronautics and Space Administration.
INVESTIGATION OF THERMAL SHOCK RESISTANCE OF ZIRCONIA WITH METAL ADDITIONS. Alan Arias.
September 1964. ii, 72p. OTS price, $2.00.
(NASA TECHNICAL NOTE D-2464)

Thermal shock resistances of compositions of ZrO_2 with 15 mole precent Ti prepared by various methods as well as that of stabilized zirconia were determined as a function of heat-transfer coefficient on disks with thermally insulated faces. The thermal shock resistance of one of the ZrO_2-Ti compositions was also calculated from the values of its physical properties, which were also determined. The values of thermal shock resistance obtained by both methods showed very good agreement for quenches from below the transformation range of ZrO_2. The discrepancy between the experimental and calculated values for quenches through the transformation range of ZrO_2 was traced to the elastoplastic behavior of these compositions on heating and cooling.

(over)

I. Arias, Alan
II. NASA TN D-2464

NASA

NASA TN D-2464
National Aeronautics and Space Administration.
INVESTIGATION OF THERMAL SHOCK RESISTANCE OF ZIRCONIA WITH METAL ADDITIONS. Alan Arias.
September 1964. ii, 72p. OTS price, $2.00.
(NASA TECHNICAL NOTE D-2464)

Thermal shock resistances of compositions of ZrO_2 with 15 mole precent Ti prepared by various methods as well as that of stabilized zirconia were determined as a function of heat-transfer coefficient on disks with thermally insulated faces. The thermal shock resistance of one of the ZrO_2-Ti compositions was also calculated from the values of its physical properties, which were also determined. The values of thermal shock resistance obtained by both methods showed very good agreement for quenches from below the transformation range of ZrO_2. The discrepancy between the experimental and calculated values for quenches through the transformation range of ZrO_2 was traced to the elastoplastic behavior of these compositions on heating and cooling.

(over)

I. Arias, Alan
II. NASA TN D-2464

NASA

NASA TN D-2464
National Aeronautics and Space Administration.
INVESTIGATION OF THERMAL SHOCK RESISTANCE OF ZIRCONIA WITH METAL ADDITIONS. Alan Arias.
September 1964. ii, 72p. OTS price, $2.00.
(NASA TECHNICAL NOTE D-2464)

Thermal shock resistances of compositions of ZrO_2 with 15 mole precent Ti prepared by various methods as well as that of stabilized zirconia were determined as a function of heat-transfer coefficient on disks with thermally insulated faces. The thermal shock resistance of one of the ZrO_2-Ti compositions was also calculated from the values of its physical properties, which were also determined. The values of thermal shock resistance obtained by both methods showed very good agreement for quenches from below the transformation range of ZrO_2. The discrepancy between the experimental and calculated values for quenches through the transformation range of ZrO_2 was traced to the elastoplastic behavior of these compositions on heating and cooling.

(over)

I. Arias, Alan
II. NASA TN D-2464

NASA

NASA TN D-2464
National Aeronautics and Space Administration.
INVESTIGATION OF THERMAL SHOCK RESISTANCE OF ZIRCONIA WITH METAL ADDITIONS. Alan Arias.
September 1964. ii, 72p. OTS price, $2.00.
(NASA TECHNICAL NOTE D-2464)

Thermal shock resistances of compositions of ZrO_2 with 15 mole precent Ti prepared by various methods as well as that of stabilized zirconia were determined as a function of heat-transfer coefficient on disks with thermally insulated faces. The thermal shock resistance of one of the ZrO_2-Ti compositions was also calculated from the values of its physical properties, which were also determined. The values of thermal shock resistance obtained by both methods showed very good agreement for quenches from below the transformation range of ZrO_2. The discrepancy between the experimental and calculated values for quenches through the transformation range of ZrO_2 was traced to the elastoplastic behavior of these compositions on heating and cooling.

(over)

I. Arias, Alan
II. NASA TN D-2464

NASA

NASA TN D-2464

Experiments to elucidate the mechanism by which Ti improves the thermal shock resistance of ZrO_2 were also carried out.

NASA

NASA TN D-2464

Experiments to elucidate the mechanism by which Ti improves the thermal shock resistance of ZrO_2 were also carried out.

NASA

NASA TN D-2464

Experiments to elucidate the mechanism by which Ti improves the thermal shock resistance of ZrO_2 were also carried out.

NASA

NASA TN D-2464

Experiments to elucidate the mechanism by which Ti improves the thermal shock resistance of ZrO_2 were also carried out.

NASA

"The aeronautical and space activities of the United States shall be conducted so as to contribute . . . to the expansion of human knowledge of phenomena in the atmosphere and space. The Administration shall provide for the widest practicable and appropriate dissemination of information concerning its activities and the results thereof."

—NATIONAL AERONAUTICS AND SPACE ACT OF 1958

NASA SCIENTIFIC AND TECHNICAL PUBLICATIONS

TECHNICAL REPORTS: Scientific and technical information considered important, complete, and a lasting contribution to existing knowledge.

TECHNICAL NOTES: Information less broad in scope but nevertheless of importance as a contribution to existing knowledge.

TECHNICAL MEMORANDUMS: Information receiving limited distribution because of preliminary data, security classification, or other reasons.

CONTRACTOR REPORTS: Technical information generated in connection with a NASA contract or grant and released under NASA auspices.

TECHNICAL TRANSLATIONS: Information published in a foreign language considered to merit NASA distribution in English.

TECHNICAL REPRINTS: Information derived from NASA activities and initially published in the form of journal articles.

SPECIAL PUBLICATIONS: Information derived from or of value to NASA activities but not necessarily reporting the results of individual NASA-programmed scientific efforts. Publications include conference proceedings, monographs, data compilations, handbooks, sourcebooks, and special bibliographies.

Details on the availability of these publications may be obtained from:

SCIENTIFIC AND TECHNICAL INFORMATION DIVISION

NATIONAL AERONAUTICS AND SPACE ADMINISTRATION

Washington, D.C. 20546